Contact and Remote Breathing Rate Monitoring Techniques: A Review

Mohamed Ali, *Member, IEEE*, Ali Elsayed, Arnaldo Mendez, *Member, IEEE*, Yvon Savaria, *Fellow, IEEE*, and Mohamad Sawan, *Fellow, IEEE*

***Abstract*—Breathing rate monitoring is a must for hospitalized patients with the current coronavirus disease 2019 (COVID-19). We review in this paper recent implementations of breathing monitoring techniques, where both contact and remote approaches are presented. It is known that with non-contact monitoring, the patient is not tied to an instrument, which improves patients' comfort and enhances the accuracy of extracted breathing activity, since the distress generated by a contact device is avoided. Remote breathing monitoring allows screening people infected with COVID-19 by detecting abnormal respiratory patterns. However, non-contact methods show some disadvantages such as the higher set-up complexity compared to contact ones. On the other hand, many reported contact methods are mainly implemented using discrete components. While, numerous integrated solutions have been reported for non-contact techniques, such as continuous wave (CW) Doppler radar and ultrawideband (UWB) pulsed radar. These radar chips are discussed and their measured performances are summarized and compared.**

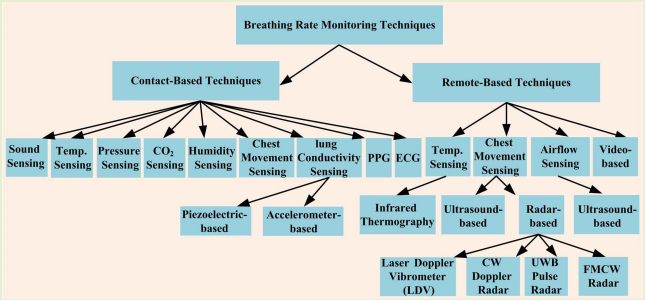

***Index Terms*—Chronic obstructive pulmonary diseases (COPD), COVID-19, breathing monitoring techniques, Doppler radar, ultra-wideband (UWB) pulse radar.**

I. Introduction

THE main function of the respiratory system is gas exchange. Oxygen is transferred from the external ambient into our bloodstream, while carbon dioxide is expelled outside [1]. Fig. 1 illustrates the respiratory system including the upper and lower respiratory tract regions. When inhaling, the air flow passes through the larynx and the trachea, and then splits into two bronchi. Each bronchus is divided into two smaller branches to form bronchial tubes. These tubes form a multitude of pathways within the lung that terminate at the end with a link to the alveoli. Gases exchanges occur at the alveoli, where oxygen diffuses into the lung capillaries in exchange with carbon dioxide. Exhalation starts after the gas exchange and the air containing carbon dioxide begins to return across the bronchial pathways back out to the external ambient through the nose or mouth. In addition, the respiratory system has other secondary functions including filtering, warming, and humidifying the inhaled air.

The respiratory rate (RR), or the number of breaths per minute, is a clinical parameter that represents ventilation, i.e., the movement of air in and out of the lungs. A change in RR is often the first sign of deterioration as the body attempts to maintain oxygen delivery to the tissues [2], [3].

An accurate measurement of the RR is essential for vital signs monitoring (i.e., RR, oxygen saturation, temperature, blood pressure, pulse/heart rate, and alert, verbal, pain, unresponsive (AVPU) response) of patients with breathing troubles such as Chronic obstructive pulmonary disease (COPD) and COVID-19. The latter, which is caused by a coronavirus, induces severe respiratory illness to many. It has a major impact on society and it is currently receiving a great deal of attention. In the same vein, SARS-CoV-2 has also been a very significant cause of concerns. Patients with moderate or severe COVID-19 are usually hospitalized for close monitoring and supportive care, where indicators of severe disease are

Manuscript received February 25, 2021; revised March 25, 2021; accepted March 26, 2021. Date of publication April 12, 2021; date of current version June 30, 2021. This work was supported in part by Natural Sciences and Engineering Research Council of Canada (NSERC), in part by Mathematics of Information Technology and Complex Systems (MITACS), and in part by Dymedso Inc. The associate editor coordinating the review of this article and approving it for publication was Prof. Tarikul Islam. *(Corresponding author: Mohamed Ali.)*

Mohamed Ali is with the Department of Electrical Engineering, Polytechnique Montréal, Montreal, QC H3T IJ4, Canada, and also with the Department of Microelectronics, Electronics Research Institute, Cairo 12622, Egypt (e-mail: mohamed.ali@polymtl.ca).

Ali Elsayed is with the Nanotechnology and Nanoelectronics Program, University of Science and Technology, Zewail City of Science, Technology and Innovation, Giza 12578, Egypt.

Arnaldo Mendez and Yvon Savaria are with the Department of Electrical Engineering, Polytechnique Montréal, Montreal, QC H3T IJ4, Canada.

Mohamad Sawan is with the Department of Electrical Engineering, Polytechnique Montréal, Montreal, QC H3T IJ4, Canada, and also with the School of Engineering, Westlake Institute for Advanced Study, Westlake University, Hangzhou 310024, China.

Digital Object Identifier 10.1109/JSEN.2021.3072607

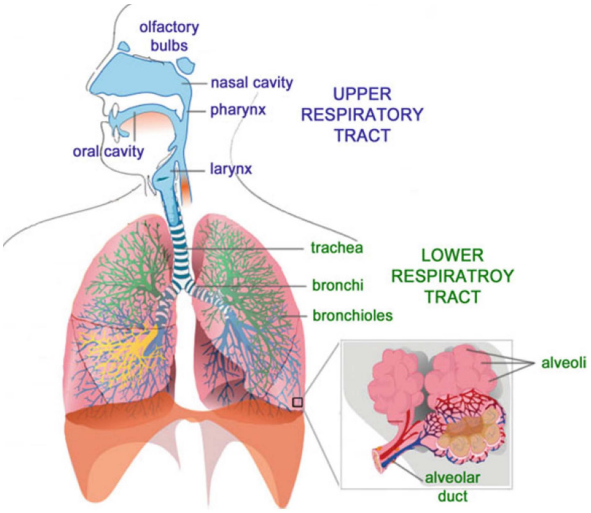

Fig. 1. Illustration of human respiratory system. [1].

marked Tachypnea (breathing rate, $\geq$ 30 breaths per minute) [4], [5]. Therefore, continuous breathing rate monitoring is required to evaluate the progress of hospitalized patients with COVID-19. In addition, remote breathing rate monitoring helps screening people infected with COVID-19 by detecting abnormal respiratory patterns [6], [7].

In addition, irregular cardiac rhythms and breathing cessation are thought to be the underlying triggers of sudden adult death syndrome (SADS) and infant sudden death syndrome (SIDS), which is the third leading cause of infant mortality [8]. Hence, continuous monitoring of respiratory rate can help minimizing life-threatening occurrences, especially for patients with respiratory and cardiovascular problems. Respiratory rates can be utilized along with breathing patterns to both diagnose and monitor a person's health conditions when it comes to pulmonary diseases. The normal respiratory rate varies from one person to another, but in general it lies between 12-20 breaths per minute at rest [9]. Abnormal respiratory rates can fall into three categories: Tachypnea (high respiratory rate), Bradypnea (low respiratory rate), or Apnea (cessation of breathing) [10]. The latter is often divided into two main categories called central, caused by respiratory system development deficiencies, and obstructive, caused by airway obstruction [11]. Other abnormal respiratory patterns such as Kussmaul's breathing, Apneustic breathing, Cheyne–Stokes respiration, Ataxic and Biot's breathing, and Agonal breathing have been reported in [12]. Ideal breathing monitoring systems should be non-invasive, comfortable, easy to use, low-cost, and should offer high accuracy.

This paper reviews recent implementations (discrete and integrated) of various respiratory monitoring techniques. These methods are classified as either contact or remote (non-contact). Contact and wearable respiratory devices have direct contact with the subject's body. On the other hand, non-contact monitoring techniques are based on measuring the respiration rate without making contact with the subject's body.

In the remaining parts of the paper, we introduce contact-based methods for respiration monitoring in Section II and non-contact approaches are presented in Section III, where the measured performance of the integrated solutions are summarized and compared. Our results and evaluation of the reviewed breathing monitoring techniques are presented in Section IV. Finally, conclusions from this review are drawn in Section V.

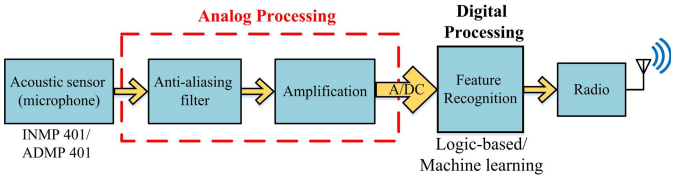

Fig. 2. Block diagram of the sound-based respiratory monitoring.

II. Contact Respiratory Monitoring Techniques

Contact respiratory devices have direct contact with the subject's body. They are based on measuring one of the following parameters: respiratory sound, respiratory airflow, respiratory-related chest, or abdominal movements.

A. Sound-Based Respiratory Monitoring

One of the oldest type of medical examinations is auscultation, in which a physician assesses circulatory, respiratory, and gastrointestinal systems by examining the internal sounds of the body. In chronic respiratory diseases such as chronic obstructive pulmonary diseases (COPD), chronic bronchitis, and bronchial asthma, futile secretions (i.e. mucus and sputum) are produced in the breathing tracts. This leads to inflammation causing airways obstruction and thus the airflow speed changes resulting in abnormal breathing sounds [13]. Decades of medical studies have established correlations between anomalous breathing sounds including wheezing, crackles, rhonchi, broncho-vesicular and bronchial, and corresponding potential diagnoses.

However, the accuracy of information obtained by auscultation depends on the experience of the physician [14]. In addition, this method does not allow continuous monitoring [14]. To overcome these limitations, wireless and wearable acoustic monitoring devices are of essence to continuously follow up with patients. Fig. 2 shows a generic block diagram of the sound-based breathing monitoring system, where the sound is captured by a microphone. Then, the signal is processed through some analog circuits for filtering and amplification purposes. The processed analog signal is then digitized by means of an analog-to-digital converter (ADC) for further digital processing, including features recognition. In addition, a wireless transmission circuit may be used to update the patient's corresponding physician and to reduce power usage by processing the data over the base station i.e. a laptop, mobile phone, or internet servers. The use of acoustic devices varies from only coughing and breathing frequency detection to full wheeze detection and analysis [15], [16]. Many devices combine the use of acoustic breathing pattern with the chest displacement pattern to enhance accuracy [15], [17]. Sound detection devices (e.g. microphone) are usually located in chest area. In [17], the strengths of the acquired acoustic signals from three locations (the left interior of the first intercostal

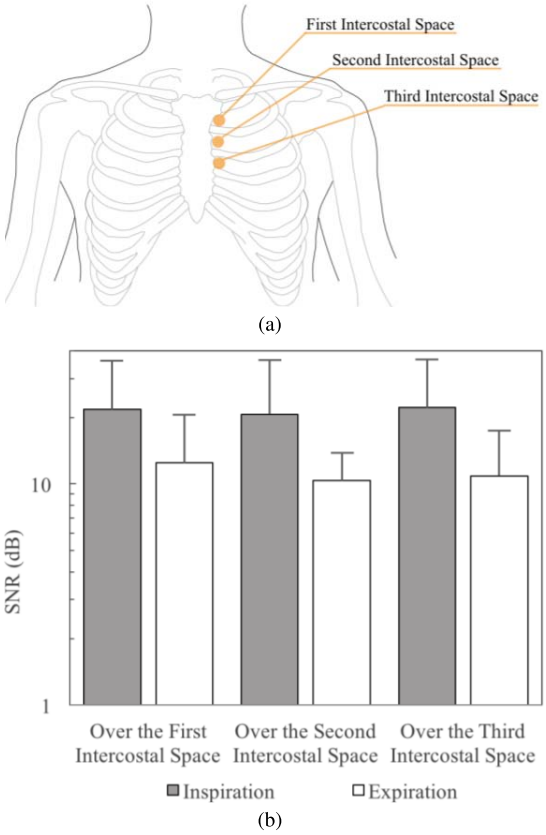

Fig. 3. (a) Possible locations for the sound detection device on the chest, and (b) Strengths of the acquired acoustic signal at each location [17].

space, the left interior of the second intercostal space, and the left margin of the third intercostal space) on the chest were compared (see Fig. 3). It was found that the acoustic signal is slightly stronger around the first intercostal space level.

To efficiently develop wheeze detection algorithms, a sufficient and reliable database for wheezing sounds is required. One of these databases was built in [18]. Other lung sounds recordings are also available online on different platforms used mainly to train medical students for auscultation. However, sufficient and reliable datasets for lung sounds other than wheezing sounds are still lacking. Another major challenge is that acoustic signals are susceptible to noise (artifacts) either from the surroundings or from other body voices, i.e. talking, coughing, and heartbeats [19]. Thus, the detection system should have high sensitivity in addition to consume low-power and be compact in order to cope with the wearable technology trends in biomedical engineering. The breathing sound analysis algorithm given in [19] archives a sensitivity of 91.51 %, while in [20], a 91.3 % success rate and relatively low-power implementation was achieved.

B. Airflow Sensing-Based Respiratory Monitoring

Respiratory rate can be extracted from airflow as expiratory air is warmer than inspiratory air. In addition, the pressure of the airflow can be used to extract the respiratory signal. To monitor patients' breathing, a sensor attached to the airways is required to measure the changes in these parameters. Moreover, the breathing activity could be extracted by detecting the expired carbon dioxide (CO_2). Furthermore, humidity sensors could be adopted to detect the breathing rate as expiratory air has higher humidity than inspiratory air.

1) Airflow Temperature Sensing: In this technique, the difference in temperature between the inhaled and exhaled air is measured by means of a thermistor located under the nose. Authors in [21], employed a small temperature resistor clipped onto the nose, and its output was fed to a high-gain differential amplifier as shown in Fig. 4(a). This amplified signal is then applied to an envelope detector. The output signal is subsequently processed by a microcontroller unit (MCU) to calculate the respiration rate. An additional temperature sensor could be used to detect the ambient temperature so that the device is usable virtually at all temperatures. Also, the airflow temperature sensing-based breathing monitoring technique was implemented using one integrated circuit (IC), TMP100, which involves a temperature sensor and an ADC to digitize the measured signal as depicted in Fig. 4(b) [22]. This work used an additional module that uses a wireless GSM modem to send urgent results to the healthcare givers.

The backscattering technique that is based on a transponder response modulation has been used for wireless communication [23], [24]. The transponder is composed of an array of dipoles, loaded with a varactor diode, which implements a frequency selective surface as shown in Fig. 4(c). The measured temperature tunes the frequency of a low-frequency oscillator. Then, the oscillator output modulates the varactor diode, which in turn modulates the backscattered response of the transponder. This method helps to reduce the power consumption since the only active element is the oscillator; no ADC or MCU are needed in the transmitter side. A customized reader is then used to receive the backscattered signal and extract the temperature readings. The maximum reading distance achieved by this method is 3 m [23]. This system is mounted on the subject's head has shown in Fig. 4(d). Although backscattered communication was used in this system to reduce power consumption, it suffers from the sensitivity to the angle and distance variations from the transponder.

2) CMOS/MEMS-Based Airflow Pressure Sensing: A micro-electromechanical system (MEMS) micro-cantilever-based respiratory airflow sensor has been presented for the first time in [29]. When the airflow is applied to the sensor, it deforms and its resistance changes accordingly. This results in a linear change in the sensor output voltage. Since MEMS sensors are compatible with CMOS processes, fully integrated systems could be realized. Authors in [25] integrated three resistive MEMS sensors together with the CMOS processing circuits in one chip as shown in Fig. 5(a). In this design, the generated output voltage from the MEMS sensor is applied first to a chopper circuit to modulate the low-frequency respiratory signals to higher frequencies. Then, a differential difference amplifier (DDA) is employed to amplify the modulated signal. Next, another chopper is used to modulate the input offset of the DDA and other noises (like flicker noise) to the high-frequency range, while the original respiratory signal is demodulated back to the low-frequency range. This structure allows filtering noise by means of a low-pass filter (LPF). Since the needed total

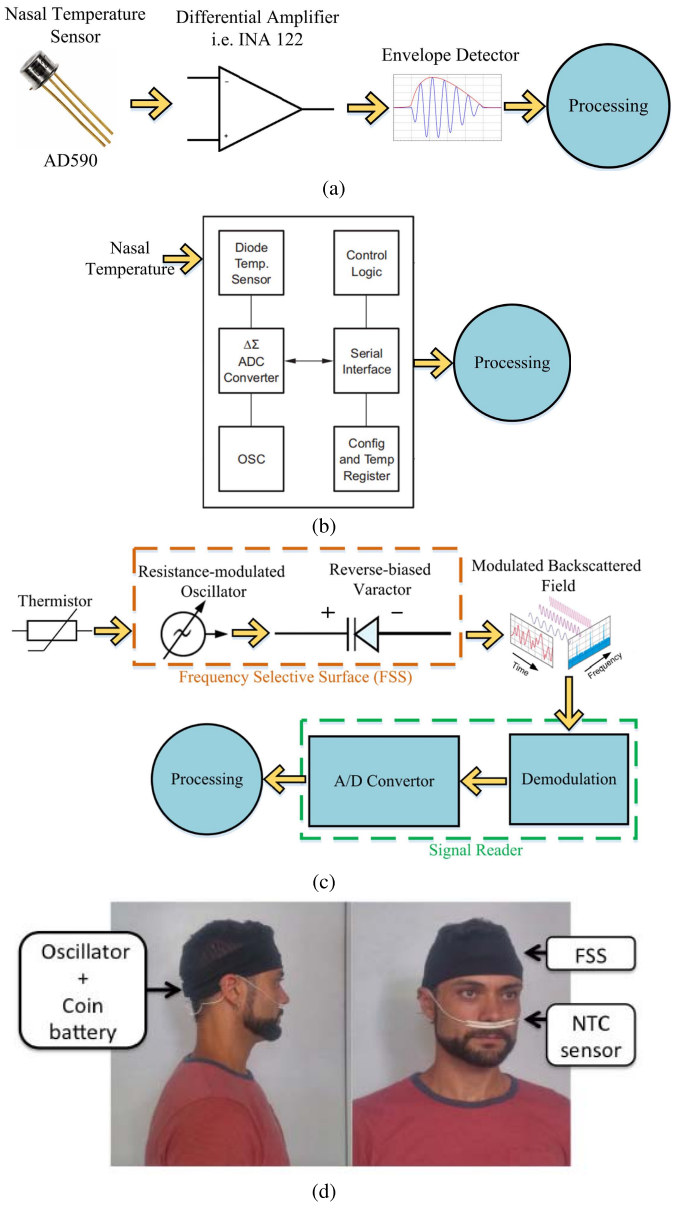

Fig. 4. Implementations of airflow temperature sensing-based respiratory monitoring: (a) Using analog components, (b) Using the TMP100 IC, (c) Backscattering approach, and (d) System's mounting on the subject's head [23].

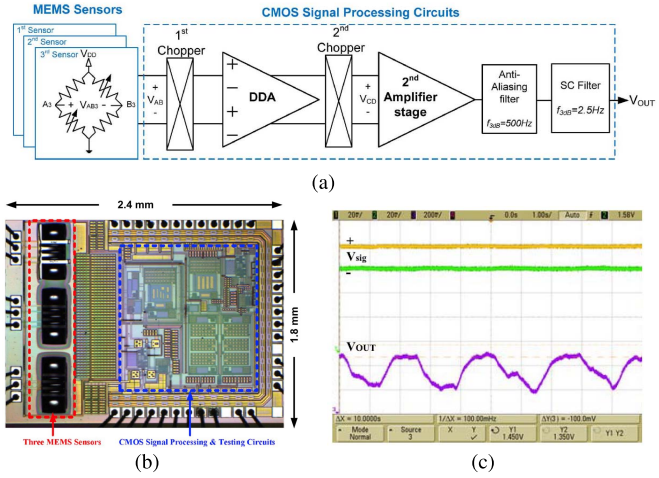

Fig. 5. CMOS/MEMS-based respiration detection system: (a) Block diagram [25], (b) Chip microphotograph [25], and (c) Measured mouth breathing airflow [26].

TABLE I
PERFORMANCE COMPARISON OF CMOS/MEMS CHIPS FOR AIRFLOW PRESSURE DETECTION

References	[25]	[26]	[27]	[28]
Technology	0.35 μm CMOS/ MEMS	0.35 μm CMOS/ MEMS	0.35 μm CMOS/ MEMS	0.5 μm CMOS
Supply Voltage (V)	3.3 and 5	3.3	3.15 – 4.5	5
Bandwidth (Hz)	2.56	4	NA	NA
Integrated MEMS sensor	Yes	Yes	Yes	No
Offset cancellation	None	DC servo loop (DSL)	Switched capacitor DSL	None
Power Cons.	NA	0.54 mW*	2.53 mW**	33 μW*
Chip area (mm^2)	4.32	4.23	4.52	0.163***

* Power of processing circuits only.
** Power of processing circuits and MEMS sensors.
*** Active area only.

gains of the three MEMS sensors may be different, a second amplifier stage is employed with an off-chip resistor to adjust its gain. A switched-capacitor (SC) circuit-based LPF with a bandwidth of 2.5 Hz was implemented. Also, an anti-aliasing filter was used before the SC filter to cancel signals with frequencies higher than half of the SC switching frequency. This work is implemented in 0.35 μm CMOS/MEMS technology with a chip area of 1.8 $\times$ 2.4 mm^2 as depicted in Fig. 5(b). However, integrated resistive MEMS sensors have DC offset as a result of inherent resistance mismatch due to process variations.

Authors in [26] implemented a DC servo loop (DSL) offset calibration scheme as part of an airflow detection CMOS/MEMS chip to automatically eliminate DC offsets in the MEMS sensors. The mouth breathing airflow measurement process exploiting this chip is illustrated in Fig. 5(c). Another fully integrated approach has been reported in [27], where it includes the MEMS sensors, analog sensing circuits, an ADC to allow further processing, and three capacitor-less low dropout voltage regulators so that the chip can be powered through a single Li-ion battery. Another similar work has been reported in [28], where an off-chip MEMS sensor has been used to detect the respiratory signal, while the processing circuits have been integrated in 0.5 μm CMOS technology with an active silicon area of 0.163 mm^2. In addition, an Artaflex wireless transceiver module has been utilized for data transmission. The performance of the CMOS/MEMS chips for airflow pressure detection to extract the breathing activity that were cited have been summarized in Table I.

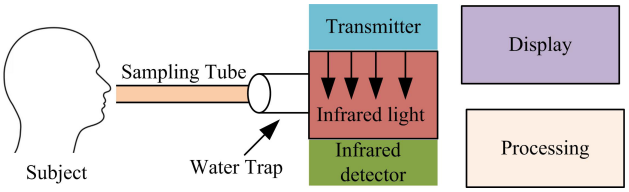

Fig. 6. Block diagram of infrared spectroscopy device.

3) CO_2 Monitoring (Capnometry): Breathing rate could be extracted be measuring the concentration of subject's expired carbon dioxide (CO_2). The Capnography method, which is the gold standard for RR measurements [30]–[33], is used for measuring patient's breathing rate in clinical studies. It continuously measures the concentration or partial pressure of CO_2 in respiratory gases, where the exhaled air contains more CO_2 than the inhaled air. Infrared spectroscopy is the most commonly used method to measure the amount of CO_2 in gas samples. With that method, a transmitter is used to emit a beam of infrared light through the gas sample. That beam falls onto an infrared detector as depicted in Fig. 6. The presence of CO_2 in the gas results in a reduction in the amount of the detected light, which results in voltage changes in the processing circuit. Although Capnography is potentially accurate, it requires sensitive CO_2 sensors to be attached to the subject through a medical face mask or nasal cannula, which results in a reduced comfort level to the patient. Various infrared carbon-dioxide sensors and their specifications have been reported in [34].

4) Humidity-Based Sensing: Since the air exhaled has higher humidity than the air inhaled, breathing rate monitoring could be done using a humidity sensor placed close to the patient's nose or mouth. Various humidity sensors could be adopted including resistive sensors [35], capacitive sensors [36], nanocrystal and nanoparticles sensors [37]–[39], fiber optic sensors [40], [41], and impedance sensors [42]. These different types of humidity sensors have been reviewed and their specifications were compared in [43]. A paper-based humidity sensor has been investigated in [39], where changes in resistance of a paper with printed graphite electrodes has been converted into an electrical signal.

As shown in Fig. 7, this compact sensor has been embedded into a medical mask. A data acquisition and processing unit has been built using off-the-shelf electronic components and supplied by a rechargeable 5V DC battery. This unit was used to apply a voltage across the paper electrodes. The resulting signal is received, amplified and digitized to produce a measurement transmitted over a wireless Bluetooth link to the display device (a tablet computer running a custom-built Android application). This cost-effective implementation was shown to be capable of continuous monitoring of breathing rate at rest and during walking (up to 60 breaths per minute). However, a facemask is required to allow measurements, which is unsuitable for patients with breathing troubles.

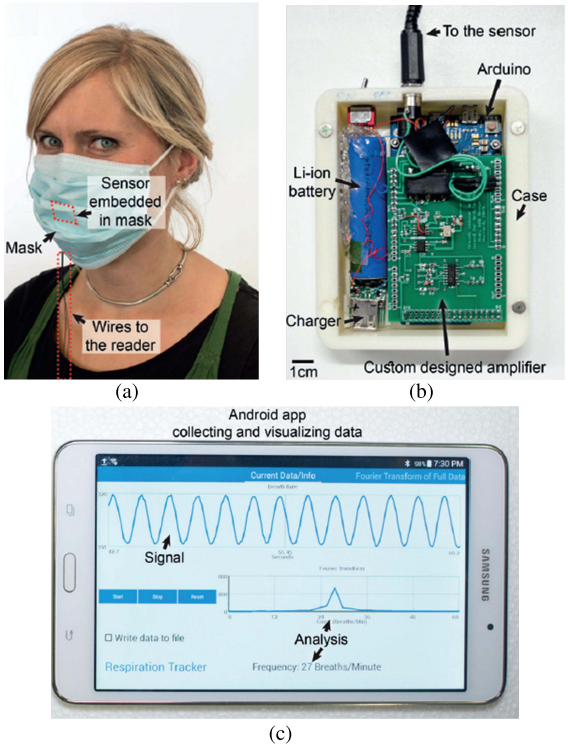

Fig. 7. Breathing rate monitoring prototype using a paper-based humidity sensor [39]: (a) A facemask with the embedded paper-based sensor, (b) Data acquisition board, and (c) Display device (A tablet computer running an Android application).

C. Chest Movement-Based Respiratory Monitoring

1) Using Piezoelectric Transducers: A thin sheet of polyvinylidene fluoride (PVDF), which is a piezoelectric material, can be used to measure the change in body volume during respiration. An array of 4 × 1 sensors reported in [48] has been designed to be placed under the subject's back (between a bed cover and a bed mattress). The measured signals are applied to an apnea detection algorithm to extract the respiratory signal among various signals generated from the PVDF and then, detect apnea. This approach needs complex setup. Authors in [44] presented a wearable solution, where integrated processing circuits have been used to receive and process the signal from the PVDF sensor. In this design, the charge generated by the PVDF sensor is firstly converted to a voltage by means of a charge amplifier and then digitized using an ADC. In addition, wireless data transmission has been implemented with an impulse radio ultra-wideband (IR-UWB) radio transmitter working in the 3.1–5 GHz frequency range. A block diagram of the system exploiting this technique and the implemented chip are shown in Fig. 8. Although this approach has many advantages including low-power integrated CMOS circuits, low weight, and wireless telemetry, it needs to be attached to a jacket or a chest belt for proper operation, which decreases the patient's comfort level.

2) Using Accelerometers: As shown in Fig. 9(a), respiration is expressed through both thoracic cage and abdominal cavity activities. So, during inspiration, the chest expands and the abdomen rises. While in case of expiration, the chest contracts and the abdomen falls. Therefore, thoracic and/or abdominal cavity motions could be monitored (by means of accelerometer and/or gyroscope sensors) to extract the breathing activity [15], [49]–[54]. Authors in [15], [49] used two sensor nodes, as shown in Fig. 9(b), to collect the thoracic and abdominal

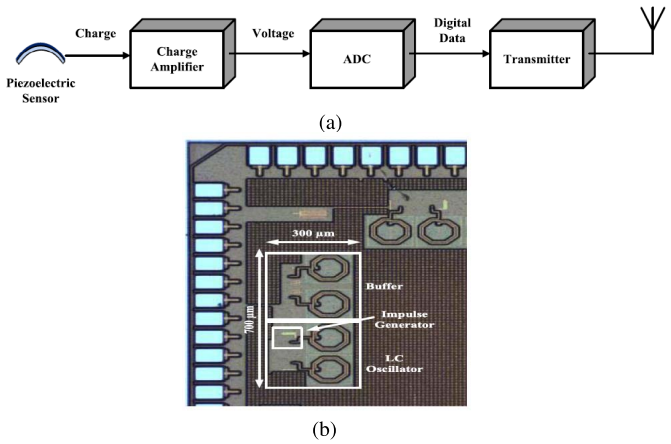

Fig. 8. Piezoelectric sensor-based breathing monitoring system [44]: (a) Block diagram and (b) Chip microphotograph.

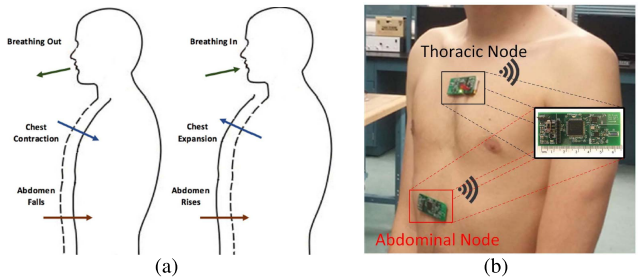

Fig. 9. (a) Chest and abdomen activities during respiration cycle [15] and (b) Two attached sensor nodes, equipped with inertial measurement units, to measure and transmit chest and abdomen motions [15].

cavity motions data. Each sensor node has an inertial measurement unit (LSM9DS0 provided by STMicroelectronics) to provide the accelerometer and gyroscope data that represent the thoracic or abdominal cavity motion. The data obtained from each inertial measurement unit is then transferred to an MCU (through an SPI interface bus) to perform angle calculations and filtering before being wirelessly transmitted to a base-station by means of a low-power radio module. The received signal is smoothed using a Savitzky-Golay smoothing filter and then applied to a peak detection algorithm to extract the breathing peaks. Although this prototype has some advantages including small size and low-weight, which allows better comfort to the person, it consumes a relatively high current (28.2 mA), that lead to an autonomy of only 6 hours when it is powered by a 100 mA-h lithium battery.

3) Ultrasound-Based; Wearable Approaches: Ultrasound waves can be used to monitor human's vital signs such as breathing and heart rates. In that class of systems, an ultrasound transmitter is used to emit ultrasound waves towards the subject's chest and the restored waves are changed either in amplitude or phase as a result of the motions of heart and respiratory systems. Ultrasound sensors can be either in close contact with the body [56] or separated [57], [58]. The rest of this section investigates the ultrasound-based wearable approaches, while the section dealing with remote-based techniques covers the ultrasound-based remote methods.

A piezo-ultrasound transducer is commonly used as it offers low cost and good performance. It is important when using ultrasound transducers to place the sensor away from the bones as they introduce both large attenuation factor and acoustic impedance of 5 dB/cm and 6×10^6 rayl, respectively [56]. The intercostal area among T5-T8 ribs offers a good resolution for monitoring both the heart and internal organs movement [55], [59]. The axial resolution of the sensor, hence, must be adjusted to accurately catch this range. This range can be calculated simply by dividing the velocity of the wave by the double of the operating frequency [56]. Although increasing the frequency improves accuracy, it also increases the power consumption and computational complexity, which are undesirable with wearable devices.

An example of wearable ultrasound-based respiratory and heart rate system is shown in Fig. 11 [55], [59]. In this implementation, a high-voltage (HV) pulser is employed to produce ± 20 V with 1 MHz pulsed signal. This HV swing is used to improve the intensity of ultrasound waves. The generated pulses are applied to the PZT-4 piezo transducer. The reflected ultrasound beams are then amplified by a two-stage linear amplifier exploiting a wide band-pass passive filter to remove the unwanted high and low frequency components of the received signal. The magnified waveform is then applied to an envelope detector and a dynamic average threshold crossing (D-ATC) circuit to simplify digital processing. A 2-channel, 8-bit ADC is utilized to digitize the received signal before applying it to an FPGA for further processing. Then, the generated data from the FPGA is logged and processed by MATLAB with a user-friendly GUI interface, where low and high-pass finite impulse response (FIR) filters have been used to extract both low (respiration) and high (heart cycles) frequency elements of the signal, respectively. The results was compared to Spirometry and showed 89 % agreement. The obtained respiratory signal has sensitivity and specificity of 94.5% and 94.0%, respectively with the spirometer signals used as reference. Despite the promising results of the contact ultrasound sensor, it has few drawbacks such as the use of both adhesive patches to stabilize the sensor and conductive material, i.e. gel, which can cause some discomfort to the patient especially for prolonged monitoring. It is also sensitive to upper body movements and prone to error in cases of shallow breathing and obstructive sleep apnea [55], [59].

D. Lung Conductivity Sensing

Bioimpedance fluctuations in the thorax can be used to monitor respiration. This concept was first introduced in [60], where a magnetically coupled device was used to measure conductivity variations in the chest as a result of breathing. In this study, a three-coil differential transformer was used. The center coil induces eddy currents into the body by exciting it with a 100 kHz sine wave signal generated by a crystal oscillator that is amplified by a power amplifier. Then, the voltage induced in the secondary coils, which correlates with respiration, is measured to monitor conductivity changes. However, this approach uses three coils which results in a complex hardware. To overcome this inconvenient, several single coil-based systems have been presented [45]–[47], [61]. A Colpitts oscillator was designed using a single flexible coil placed on the body surface, where variations in coil impedance

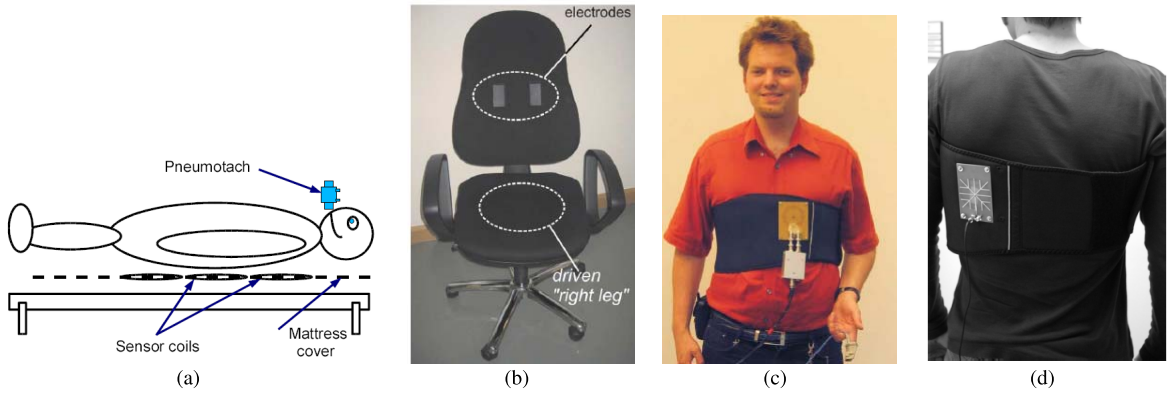

Fig. 10. Sensor (coil) locations of the impedance fluctuation sensing method: (a) In mattress cover [45], (b) Into an office chair [46], (c) In a textile carrier [46], and (d) Attached onto the body by a belt [47].

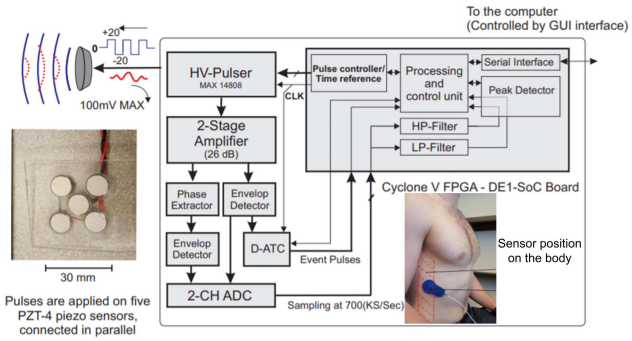

Fig. 11. A wearable ultrasound-based breathing monitoring system [55].

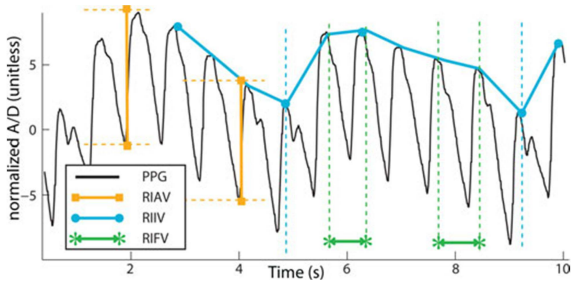

Fig. 12. Respiratory-induced variations in the PPG waveform [64].

as a result of changes in lung conductivity modulate the coil frequency [45], [61]. This frequency change is measured by a frequency counter. Although this method uses only one coil placed in a mattress under the subject, it shows inaccurate measurements when the subject moves and, as shown in Fig. 10, the coil should be attached to the subject's mattress cover, chair, cloths, or through a belt. Another conductivity sensing technique is the on body bioimpedance sensing [62]. In this technique, a bioimpedance signal is extracted using a wearable device with four electrodes attached to the patients' shoulders by injecting a current through the central arteries and trachea. The authors were able to read low and high respiratory rates with an accuracy of 100% in 10 adult subjects.

E. Photoplethysmography-Based Respiratory Monitoring

Photoplethysmography (PPG) is an optical non-invasive method used to measure blood perfusion through tissues. It is based on illuminating blood vessels with infrared light (usually through patient's finger). Then, a PPG sensor measures the amount of infrared light absorbed or reflected by blood, which reflects changes in blood volume [63]. Fortunately, breathing rate modulates the PPG waveform in three ways (as shown in Fig. 12); frequency, intensity, and amplitude [64], [65]. Firstly, the heart rate increases during inspiration and decreases during expiration, causing respiratory induced frequency variations (RIFVs) of the PPG signal. Secondly, exchange of blood between the pulmonary circulation and the systemic circulation leads to variations of perfusion baseline, called the respiratory-induced intensity variation (RIIV). Finally, the respiratory-induced amplitude variation (RIAV) is caused as a result of a reduction in cardiac output due to reduced ventricular filling. Various algorithms has been presented to estimate the BR from a measured PPG waveform, including Fourier transforms [66], digital filters [67], wavelet decomposition [68], variable-frequency complex demodulation [69], and autoregression [70].

F. Electrocardiography-Based Respiratory Monitoring

Electrocardiography (ECG) devices measure the electrical field induced by the heart and respiratory activity in the chest [71]. During the respiratory cycle, chest movements due to filling and emptying of the lungs, results in a rotation of the electrical axis of the heart, which impacts beat morphology [72].

In addition, heart rate is modulated by respiration (increases during inspiration and decreases during expiration). Furthermore, it has been shown that respiratory frequencies occur in the ECG spectrum due to heart movement [73]. Several ECG-derived respiration (EDR) techniques have been proposed to extract the breathing activity from the recorded ECG. Some of these techniques extract the breathing information through respiration-induced variations in beat-to-beat morphology [74], [75], while others extract it from the heart rate [76], [77].

III. Non-Contact Breathing Monitoring Techniques

In non-contact respiratory monitoring techniques, the device does not contact the patient's body. These methods may be

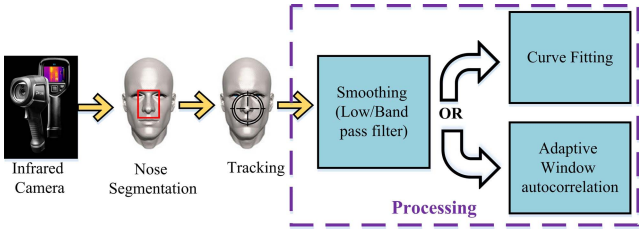

Fig. 13. Block diagram of the infrared thermography-based breathing monitoring.

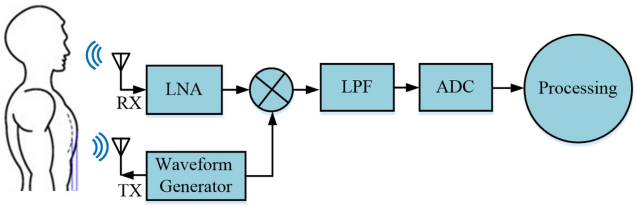

Fig. 14. Typical continuous wave CW doppler radar for vital sign detection.

more suitable in some critical settings, including the current COVID-19 pandemic and with children. In these techniques, remote monitoring could be used to screen people who are infected with COVID-19 by detecting abnormal respiratory patterns. However, non-contact techniques need complex and costly installation. In the following sections, we present in detail various techniques used to implement non-contact respiratory monitoring.

A. Camera-Based Respiratory Monitoring

1) Infrared Thermography: Since the temperature around the nostrils fluctuates during the respiratory cycle (e.g. 31.17 °C during inspiration and 31.44 °C during expiration [78]), infrared thermography can be used to monitor breathing rate. As shown in Fig. 13, infrared thermography consists of three main steps; identification of a region of interest (ROI) i.e. the nose, tracking the ROI, and extracting the breathing rate via processing. Various methods have been used to identify the ROI such as segmentation [79]–[81], classification [82], or depth maps extraction [83].

Authors in [80] and [82] adopted a tracking algorithm, while in [84], a camera combined an infrared sensor has been mounted on a tilt-platform in attempt to reduce the computation power used in segmentation and tracking. Processing is usually done after the signal is applied to a low-pass filter to remove the noise. Autocorrelation and curve fitting are the most common techniques used to process the filtered signal [81], [84], [85]. An algorithm to extract respiration signals based on pixel time series has been presented in [86], where it does not need nose-tracking and image segmentation. In addition, a depth camera was used to collect depth images of a subject (chest, abdomen, and shoulder) at 1-4 m from the depth camera [6]. Then, these images are processed to extract the respiratory signal. Authors in [7] extracted breathing signals of the video obtained from a thermal camera. Normal and abnormal breathing patterns were classified from such video through a deep learning neural network.

Even if infrared thermography can be very helpful for medical robotics and sleep study applications, it is computationally intensive and relatively expensive. Also, it is prone to error due to tracking inaccuracies in highly mobile subjects. In [78], the ability of the presented method to extract breathing rate during head motion and breathing disorders was reported. Breathing through both mouth and nose can be a source of error too if segmentation does not cover the mouth.

2) Video-Based: Breathing activity could be extracted from analyzing motions in different ROIs captured by a video camera. In [87], a charged-coupled device (CCD) camera was used to extract remotely the breathing activity due to detecting the optical flow of surface movement of the body during respiration. In [88], the breathing signal was obtained by using two CCD cameras and two fiber grating (FG) three dimensional (3D) vision sensors to detect volume changes in the location caused by respiratory rhythms. Other studies used depth image sensing cameras exploiting time-of-flight (ToF) sensors [89] or Kinect sensors [90]. In [89], a camera exploiting time-of-flight (ToF) sensors was adopted to compute a dense estimation of the 3D respiratory motion of a patient. With this method, a dense 3D surface model of patient's chest and abdomen was acquired at more than 15 frames per second. However, depth image sensing cameras have short detection ranges in addition to their high associated costs [91], [92]. In other study [91], a monochrome camera was used to track the respiratory signal and non-respiratory motions. Then, a classifier was adopted to select only the correct breath measurements. The authors in [93] presented a generic blind deconvolution technique to obtain breathing signals from videos by modeling every pixel in the abdominal-thoracic region as the output of a linear time-invariant (LTI) channel connected in parallel with an unknown dynamics response.

B. Radar-Based Respiratory Monitoring

During breathing, both the chest and abdomen move. These movements range from 4 mm to 12 mm based on each individual and the amount of inspired air [96]. Based on this concept, many contactless monitoring techniques could be used to extract the breathing rate. Continuous wave (CW) doppler radar is one of these methods, where RF signals are transmitted and then modulated by chest and abdomen movements. Also, short pulses could be transmitted towards the target and the reflected ones are then received and processed, where the time delay between the transmitted pulse and the received echo is thus proportional to the distance between the target and the radar. The latter is known as ultra-wideband (UWB) pulse radar. In the following subsections, we provide a deep review on these two radar types and highlight the main differences between them. In addition, the measured performance of the integrated solutions for radar-based respiratory monitoring are summarized and compared.

1) CW Doppler Radar: Fig. 14 presents the block diagram of a typical CW doppler radar for vital sign detection. In this technique, a carrier is transmitted toward a human body, where its frequency or phase is modulated by the physiological movement (i.e., heartbeat and respiration). By comparing the transmitted and the received signals (by means of a mixer), the change in frequency and phase can be derived from the

TABLE II
PERFORMANCE COMPARISON OF CW DOPPLER RADAR CHIPS (VALUES OBTAINED IN RESEARCH LABS SETTINGS)

Ref.	Architecture	Integration	Freq. (GHz)	Technology	Chip area (mm^2)	Output power (dBm)	Power Cons. (mW)	BR (breaths per minute)	Max. BR range (m)
[101]	Double-Sideband	TX+RX	5	0.18 μm CMOS	NA	-12	75.6	17	2
[102]		TX+RX	1.6	0.25 μm CMOS	14	6.5	NA	NA	0.5
[96]		RX	5.8	0.13 μm CMOS	1.44	NA	NA	14	3
[103]	Direct Conversion	TX+RX	2.4	0.25 μm CMOS	12.92	1	100	12.8	2
[104]		TX+RX	60	90 nm CMOS	4	3	217	24	0.75
[105]		TX+RX	60	90 nm CMOS	4.68	3	243	24	1.2
[106]	Circularly Polarized	RX	24	6-in InGaP/ GaAs	3.93	NA	NA	21	0.5
[100]	Hetero-dyne	TX+RX	60	90 nm CMOS	2.26	1	377	15	0.3
[107]	Self-Injection	TX+RX	5.8	65 nm CMOS	0.3	-8	10	10	3

received signal. The resulting baseband signal is then filtered and converted into digital form by means of an ADC for post processing to extract various features, mainly the breathing rate.

Several architectures have been presented to implement CW doppler radar including homodyne [97], heterodyne [98], double-sideband [99], direct IF sampling [94], [100]–[103], circularly Polarized [104], and self-injection locking [105]. These architectures and their baseband signal processing have been reviewed in [106]. We summarize and compare the measured performance of the integrated CW doppler radar chips in Table II. As shown in this table, the listed designs achieve different performance parameters such as operating frequency, silicon area, power consumption, breathing rate, and detection range. The ability of radar designs listed in Table II to detect the breathing rate was validated in research laboratories environment. Also, few authors compared the breathing rate obtained from a radar with that found from a reference method. For example, breathing rates obtained with the radar sensor reported in [101] were compared with those found using a piezoelectric respiratory effort belt. The authors reported a 95% match.

Front-end architecture must be carefully selected to maximize the sensitivity and extend the detection range. Fig. 15(a) shows an example of a direct conversion 5.8 GHz radar receiver chip integrated in 130 nm CMOS technology [94]. The baseband signal and spectrum detected using this chip are depicted in Fig. 15(b).

2) Laser Doppler Vibrometer (LDV)-Based Radar: Laser Doppler Vibrometer (LDV) is an optical and non-contact technique used to measure surface velocity and displacement on the basis of the Doppler shift. It adopts laser radar (instead of radio-frequency radar) to obtain the shift in laser frequency as a result of movements of the surface of interest.

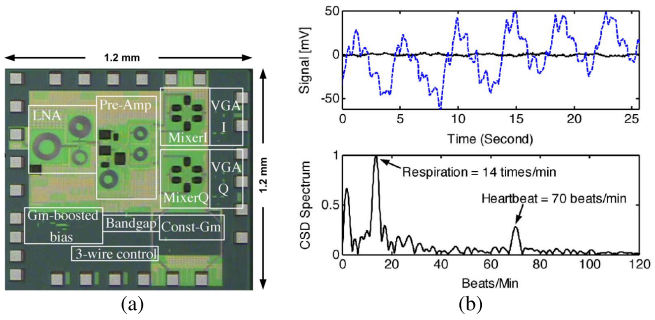

Fig. 15. A direct conversion 5.8 GHz radar receiver [94]: (a) Integrated chip in 130 nm CMOS technology and (b) Detected signals.

This approach was used to monitor breathing activity by measuring displacements of the chest-wall [107]–[110]. The LDV-based non-contact breathing rate monitoring system proposed in [109] was operated at a distance of 1.5 m, on different points of the patients' thoracic and abdominal area. Another LDV method was proposed in [110] to monitor breathing activity of preterm infants. LDV-based systems offer high sensitivity (high displacement resolution) and they require low-power density (less than 1 mW), which implies no biological impacts on patients [110]. However, they are highly affected by motion artifacts and subjects' movements in addition to their associated high cost [92], [111].

3) UWB Pulse Radar: The ultra-wideband (UWB) frequency range that extends from 3.1 to 10.6 GHz is free from interference, except for the Wi-Fi at 5 GHz. UWB systems offer some benefits over narrowband systems, including low implementation complexity, good immunity to both noise and multi-path fading, low power dissipation, and better coexistence with other existing narrowband links [122]. Since its transmitted

TABLE III
PERFORMANCE COMPARISON OF UWB PULSE RADAR CMOS CHIPS (VALUES OBTAINED IN RESEARCH LABS SETTINGS)

Ref.	Architecture	Integration	Freq. (GHz)	Technology (CMOS)	Chip area (mm^2)	Output power	Power Cons. (mW)	BR (breaths per minute)	Max. BR range (m)
[97], [115]	Correl-ation	TX+RX	3-5	90 nm	2	NA	73.2	24	0.45
[116]	Direct sampling	TX+RX	3-10	0.13 μm	2	-1.5	20	20	0.5
[117]	DS (Equivalent time method)	TX+RX	0.8-5	0.13 μm	11.88	NA	695	NA	0.75
[118]		TX+RX	6.1-8.4	90 nm	4	-13.3	120	22.27	1.3
[119]		RX	NA	65 nm	1.82	NA	76	NA	15
[120]		TX+RX	3-5	0.13 μm	3.27	3	25	12.6	10
[121], [122]	DS (swept-threshold method)	TX+RX	7.29 and 8.748	55 nm	NA	6.4	118.1	16	9

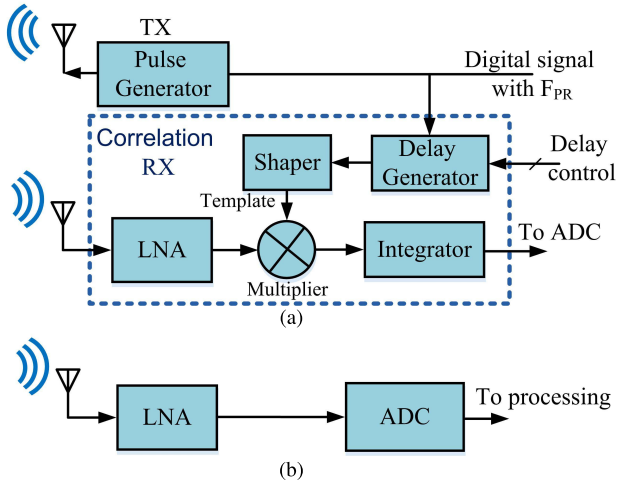

Fig. 16. UWB pulse radar: (a) Correlation receiver [95] and (b) Direct sampling receiver.

power is low (<–41.3 dBm/MHz), it has no harmful effects on human body. The main drawback of UWB link is the limited coverage. Based on this promising technology, UWB pulsed radars have been developed, where narrow pulses are transmitted with a wide instantaneous bandwidth. However, with this wide bandwidth, receiver architectures for narrowband systems cannot be used. One solution is the correlation receiver [95], [113], [123] shown in Fig. 16(a), where short pulses are produced by the pulse generator and transmitted towards the target. The reflected signals are first applied to a low-noise amplifier (LNA) to be amplified and then multiplied with a template signal that is a delayed replica of the transmitted pulses produced by means of a Shaper. The resulting signal from the multiplier is then integrated to increase the signal-to-noise ratio (SNR) and get the envelope holding the information on the movement rate. The time delay between the transmitted pulse and the received echo is thus proportional to the distance between the target and the radar. An approach based on correlations allows sampling the signal at a rate lower than the bandwidth of the actual signal. However, to track and detect objects, the delayed pulses must be swept in the range of interest, which results in complex downstream processing and control logic.

Directly sampling the signal at RF frequency is another approach (see Fig. 16(b)), which preserves all the information carried in the received waveform in the digital domain [114]–[117], [119], [120], [124], [125]. This relaxes the selection of subsequent processing and detection algorithms. However, this method results in higher power consumption and hardware complexity, since a high sampling rate is required. To solve this issue, non real-time sampling techniques like equivalent time sampling (ETS) [115]–[117], swept-threshold (ST) sampling [119], and time-extension [124] method can be utilized because the target moves slowly. Table III compares the measured performance of various UWB pulse radar chips. Unlike CW radars, no frequency conversions are needed in UWB pulse radar transceivers, which results in lower hardware complexity, leading to lower power consumption for longer battery autonomy.

4) FMCW Radar: Another method that has shown potential for remote healthcare applications is the frequency-modulated continuous-wave (FMCW) radar. Fig. 17(a) shows the principle of operation of a FMCW radar, where the frequency shifts (Δf) of the emitted radar signals over time allow determining the distance to the patient [126]. The breathing or movement of the patient changes the amplitude of the reflected waveform. Therefore, breathing activity is detected by measuring the distance between the chest wall and the transceiver device. FMCW requires very high bandwidth since the chest displacements are in millimeters [127]. On the other hand, the FMCW wide-band radar can be compact and light weight, while consuming less power, and allowing real time processing [128].

In [112], a 24 GHz FMCW radar prototype with 250 MHz bandwidth has been implemented to detect the vital signs of multiple adjacent subjects. Fig. 17(b) shows the measured range estimation for two subjects at a distance of 100 cm

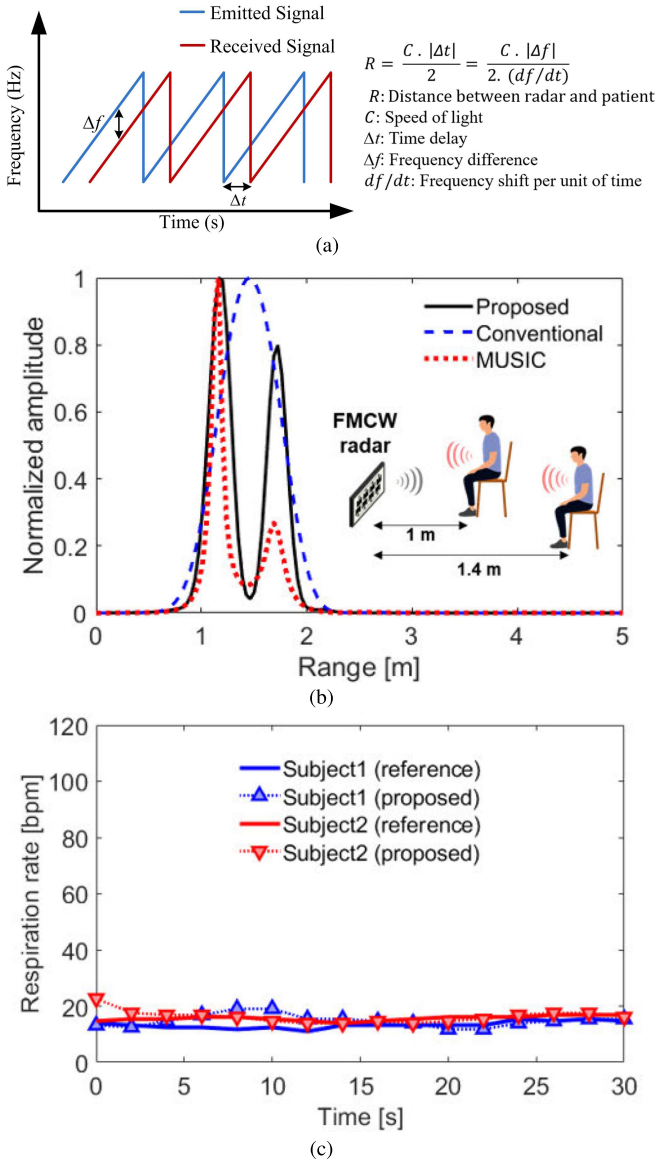

Fig. 17. FMCW radar: (a) Principle of operation, (b) Measured range estimation for two subjects at a distance of 100 cm and 140 cm [112], and (c) Measured respiration rate of these two subjects [112].

and 140 cm, while the measured respiration rate of these two subjects is illustrated in Fig. 17(c).

5) Processing Algorithms: Common processing algorithms used in research are fast Fourier transform (FFT) [129], wavelet analysis [130], and time-frequency analysis [131]. Signal processing methods like the one reported in [132] uses a combination of various algorithms to judge the signal in different situations adding to the adaptability of the algorithm and its robustness. FFT takes the DFT of the signal for a given time window and selects the dominant frequency components. On the other hand, wavelets were used to detect the breathing pattern, hence, various wavelet formulas such as continuous wavelet transform (CWT) [133] and 8^{th} order Gaussian pulse [134] have been used to model the signal in order to extract features of interest.

Other algorithms detect zero-crossing used to estimate the breathing rate based on counting negative-to-positive transitions in the obtained signal. Linear predictive coding (LPC) [135] builds a linear relationship using the least-square error method for a given time-window, then, this relationship plays the role of a filter and it is used to determine the location of the dominant spectral shape and least-squares harmonic (LSH), which uses the Geortzl algorithm in order to model the breathing pattern using a finite sum of harmonics [132].

Combining several algorithms enhances the accuracy of estimating the breathing rate [136]. However, for retrieving the whole breathing pattern for tidal volume studying, continuous wavelet transform is better equipped to do so since it provides time-frequency analysis, which helps extracting many features such as energy, entropy, frequency distribution, and power along with patterns recognition techniques for characterising the breathing disorders in addition to filtering-out the motion artefacts [133]. It is of interest that wavelet analysis is less prone to the errors caused by non-periodic breathing patterns [133], [134].

C. Ultrasound-Based: Contactless Approaches

Contactless ultrasound implementations [57], [58], [121], [137] are more suitable for sleep studies and apnea detection. It is mainly used to calculate the breathing rate and offers no discomfort to the patient. First, the distance at which the sensor is located from the subject is determined using the attenuation characteristics of the sensor [58]. The processing includes smoothing the signal, mainly using low-pass filters adjusted at the average respiration frequency, which is around 0.25 Hz. Then, various methods can be applied for peak detection such as phase portrait reconstruction [58]. Finally, phase detection is used to distinguish artifacts of non-respiratory and caretakers motions. Detection of these movements can be used to assess caretakers effort, detect seizures and determine sleep state [139]. A 40kHz self-injection-locked (SIL) ultrasound radar to detect heartbeat and respiration activities was presented for the first time in [121]. This design involves a phase-canceling feedback demodulation topology to extract the movements of the target, which greatly improves the linearity of the SIL radar. This allows the detection of large body movements and lung movements without significant distortion to the respiration and heartbeat signals. The reported prototype was tested to detect the movements of the chest at a distance of 30 cm. Resulting time-domain and the frequency-domain plots of the chest movements recorded over one-minute are provided in Fig. 18(a) and Fig. 18(b), respectively, where small involuntary body movements, breathing pattern, and heartbeat have been detected.

The work in [138] showed a method depending on air-flow measurements, where the presented system measures the frequency shift resulting from the velocity difference between the exhaled air flow and the ambient environment. In this design, a 40 kHz ultrasound transducer is placed at a distance of 50 cm above the patient head, where it emits a signal with 100 dB/0.0002 μbar emission level and 6 dB beamwidth. Then, the reflected ultrasound wave is collected by an ultrasound receiver, placed at a distance of 30 cm from the patient head. The resulting signal is subject to amplification and shaping before it further processed for visualization. The

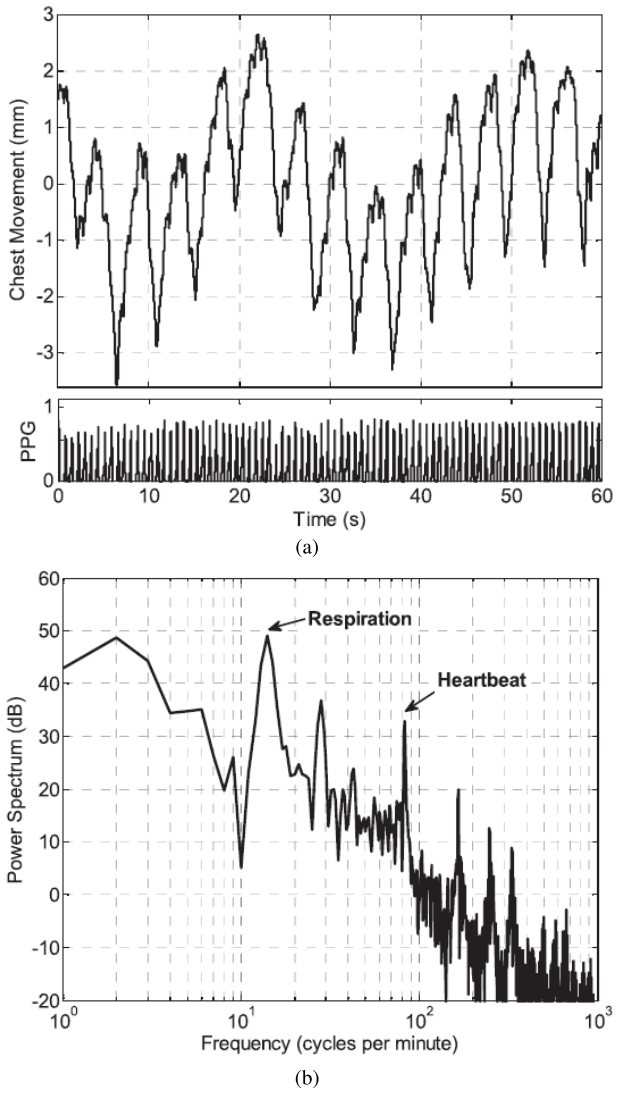

Fig. 18. Detected chest movement signals through self-injection-locked ultrasound radar represented in [121]: (a) Time-domain and (b) Frequency-domain.

results obtained with this method showed that the inclination of the subject's head affects the signal intensity. In addition, the resulting breathing signal is embedded in the doppler shift during rapid subject movements, such as sleeping position changes, which affects the detection of breathing activity.

D. Remote Plethysmography

Remote plethysmography could be done using mobile phones cameras which allows monitoring blood volume changes based on variations in the recorded light intensity [140]–[143]. It is based on using an imaging array instead of a single photo detector as in the case of contact plethysmographic sensor. One example of plethysmographic imaging was reported in [143]. This study showed the feasibility of estimating the BR by placing a finger on a mobile phone camera. Firstly, a video is recorded with the camera once a finger is correctly placed on the lens followed by detecting the optimal region of interest (ROI) from the red channel of the video. Then, a proposed algorithm extracts the imaging photoplethysmogram from this ROI, and calculates the position and amplitude of the measured pulses.

IV. Results

Several breathing rate monitoring techniques were presented in this paper. Each method offers some advantages and also suffers from some limitations as summarized in Table IV. Non-contact monitoring techniques including infrared thermography, radar-based, and ultrasound-based allow remote breathing detection, which results in improved patient's comfort compared to contact methods in which the patient is tied to an equipment. These methods, however, require a complex and static setup in addition to their susceptibility to target movements (artifacts), which affects the monitoring accuracy. On the other hand, sound detection-based breathing monitoring allows a wearable solution, in which the breathing signal could be measured without restricting much the patient's motion. However, the measured sound signal is highly susceptible to noise either from the surroundings or from other body voices, including talking, coughing, and heartbeats.

The hardware required to implement radar-based breathing monitoring systems is fairly simple, which is particularly useful in medical conditions that require continuous monitoring such as sleep studies and apnea monitoring. Radar-based systems are also immune to environmental changes coming from light and temperature. In addition, they are less computationally expensive than thermography-based approaches, which implement complex segmentation and tracking algorithms. However, radar-based breathing monitoring systems suffer from several disadvantages such as sensitivity to the target distance (the closer the distance to the transmitter-receiver pair, the higher the error [132]) and the so-called null-point problem. Other sources of errors include noise coming from subject movements and activities, artifacts from metal objects, and the existence of more than one person in the same location of observation.

CW Doppler and UWB radars are shown to have comparable performance. Both techniques are simple and allow low power consumption while offering limited detection range. CW radars suffer from clutter noise, micro-Doppler scattering resulting from other parts of a body (e.g., arm and leg), and multiple-target identification [106]. On the other hand, FM-CW radars have shown their ability to localize targets from some distance [144]. Thus, FMCW radars could be adopted for patients and elderly care in smart homes and ambulatory environments, where the subjects could be very mobile.

Although ultrasonic technology allows remote breathing monitoring, it requires a fixed setup. Also, the obtained results from this method are affected by subjects' movements, inclination of the subject's head, and sleeping position changes. CMOS/MEMS-Based airflow pressure sensing is a promising technique, where both the pressure sensor (MEMS sensor) and the CMOS processing circuits are fabricated in a single chip. This fully integrated solution achieves low power, which allows a battery-powered solution. However, it suffers from the associated fabrication cost due to the large required silicon area by the MEMS sensors. In addition, its

TABLE IV
OVERVIEW OF THE REVIEWED BREATHING MONITORING SYSTEMS

Method	Integrated solutions	Measuring parameter	Installation on the body	Comfort level	Pros	Cons	Ref.
Sound detection	No	Airflow sound	Direct contact	High	Allows detection with freely behaving user; Allows wireless telemetry	Complex hardware; Lower accuracy; Lack of reliable dataset for lung sounds; Susceptible to noise	[15]–[17], [19], [20]
Temp. sensing	No	Airflow Temp.	Direct contact	Low	Simple hardware implementation	Lower comfort level (temperature sensor in or in front of nasal/oral region)	[21]–[24]
CMOS MEMS-Based	Yes	Airflow pressure	Direct contact	Low	Fully integrated solutions (allows low power and weight)	High cost	[25]–[28]
CO_2 Sensing	No	CO_2 in airflow	Direct contact	Low	High-level of accuracy, allows continuous measuring of breathing rate in clinical studies	Requires a medical facemask or nasal cannula, which results in a lower comfortable level	[30]–[33]
Humidity Sensing	No	Humidity of airflow	Direct contact	Low	Low cost, allows continuous monitoring	The sensor should attach to a facemask or nasal cannula, which results in a lower comfortable level	[35]–[41]
Using Piezoelectric Transducers	Yes	Chest movement	On a dress or a bed mattress	Low	Allows low-power CMOS circuits, low weight, and wireless telemetry	Needs to be attached to a bed mattress, jacket, or chest belt; Lower patient's comfort level	[44], [48]
Using Accelerometers	No	Chest movement	Direct contact	Low	Small size and low-weight; Allows wireless telemetry	High power consumption; Needs to be attached directly to subject's chest and abdomen	[15], [49]–[54]
Impedance Fluctuation Sensing	No	conductivity changes of the lungs	On a dress or chair	High	Low cost hardware implementation; Both breathing and heart activity could be monitored	Needs to be attached with subject's mattress, chair, or clothes; Affects by subject moves and sensor position	[45]–[47], [62], [63]
Infrared Thermography	No	Airflow Temp.	Without contact	High	Allows remote detection; Helpful for medical robotics and sleep study applications	Complex segmentation and tracking algorithms; Relatively expensive; Prone to error due to tracking inaccuracies in highly mobile subjects	[78], [80], [81], [83], [84], [86]
Radar-based	Yes	Chest movement	Without contact	High	Allows integrated solutions; Low power; Immune to environmental changes such as light and temperature	Requires a static setup; Sensitivity to the target distance; null-point problem; Subjects to noises from subject movements and activities, artifacts from metal objects, and the existence of more than one person in the same location of observation	[94], [95], [98]–[105], [113]–[117], [119], [120]
Ultrasound-based	No	Chest movement or velocity of exhaled airflow	Direct or without contact	High	Allows remote solution	Affected by subject movements, inclination of the subject's head, and sleeping position changes	[55], [56], [57], [58], [121],[137],[138]

ability to monitor breathing for a moving target was not yet evaluated.

In general, for biosecurity (e.g. to prevent cross-contamination) and ergonomic reasons (e.g. patient's comfort

and ease of use), non-contact or remote techniques may be the best suited for continuous breathing monitoring of hospitalized patients, while for diagnosis of breathing troubles, the most accurate techniques should be used regardless whether they are implemented with contact or remote sensors.

To the best of the authors' knowledge, only the thermal imaging technique has been presented for screening people who are infected with COVID-19 by detecting abnormal respiratory patterns [6], [7]. We believe that radar-based breathing monitoring could also be considered for screening people who are infected with COVID-19, since it shows many advantages including the remote detection and immunity to environmental changes such as light and temperature. Thus, it could be used outside an hospital environment, which helps in screening large scale of people. Also, unlike infrared thermography-based breathing monitoring, radar-based could be used to screen people wearing masks. Moreover, radar-based monitoring allows a wider detection range compared to that achieved by the ultrasound-based method.

V. Conclusion

Implementation techniques for both contact and non-contact breathing monitoring have been reviewed in this paper. Non-contact monitoring methods have several advantages over contact methods, including improved patients' comfort, especially for long-term monitoring, because patients are not tied to an instrument. Moreover, the distress generated by a contact device (e.g. a mask) may alter the breathing rate. Sensitivity to environmental changes such as light and temperature is avoided in non-contact techniques, which results in better accuracy. We confirmed through this review that remote breathing monitoring allows screening of people infected with COVID-19 by detecting abnormal respiratory patterns. However, non-contact methods are more complex compared to contact ones and are affected by target movements. Finally, we evaluated various breathing monitoring systems, to identify their respective advantages and limitations.

References

[1] J. Tu, K. Inthavong, and G. Ahmadi, *Computational Fluid and Particle Dynamics in the Human Respiratory System*. Dordrecht, The Netherlands: Springer, 2013.

[2] G. B. Smith, D. R. Prytherch, P. E. Schmidt, and P. I. Featherstone, "Review and performance evaluation of aggregate weighted 'track and trigger' systems," *Resuscitation*, vol. 77, no. 2, pp. 170–179, May 2008.

[3] C. A. Alvarez *et al.*, "Predicting out of intensive care unit cardiopulmonary arrest or death using electronic medical record data," *BMC Med. Informat. Decis. Making*, vol. 13, no. 1, pp. 1–11, Dec. 2013.

[4] R. T. Gandhi, J. B. Lynch, and C. del Rio, "Mild or moderate COVID-19," *New England J. Med.*, vol. 383, pp. 1757–1766, Oct. 2020.

[5] M. Cascella, M. Rajnik, A. Cuomo, S. C. Dulebohn, and R. Di Napoli, "Features, evaluation and treatment coronavirus (COVID-19)," in *Statpearls*. Island, FL, USA: StatPearls, 2020.

[6] Y. Wang, M. Hu, Q. Li, X.-P. Zhang, G. Zhai, and N. Yao, "Abnormal respiratory patterns classifier may contribute to large-scale screening of people infected with COVID-19 in an accurate and unobtrusive manner," 2020, *arXiv:2002.05534*. [Online]. Available: http://arxiv.org/abs/2002.05534

[7] Z. Jiang *et al.*, "Combining visible light and infrared imaging for efficient detection of respiratory infections such as COVID-19 on portable device," 2020, *arXiv:2004.06912*. [Online]. Available: http://arxiv.org/abs/2004.06912

[8] P. K. Capp, P. L. Pearl, and D. Lewin, "Pediatric sleep disorders," *Primary Care, Clinics Office Pract.*, vol. 32, no. 2, pp. 549–562, 2005.

[9] K. E. Barrett, *Ganong's Review of Medical Physiology*, vol. 1. New York, NY, USA: McGraw-Hill, 2019.

[10] E. Martin, *Concise Colour Medical Dictionary*. Oxford, U.K.: Oxford Quick Reference, 2015.

[11] D. P. White, "Pathogenesis of obstructive and central sleep apnea," *Amer. J. Respiratory Crit. Care Med.*, vol. 172, no. 11, pp. 1363–1370, 2005.

[12] G. Yuan, N. A. Drost, and R. A. McIvor, "Respiratory rate and breathing pattern," *McMaster Univ. Med. J.*, vol. 10, no. 1, pp. 23–25, 2013.

[13] Y. Nagasaka, "Lung sounds in bronchial asthma," *Allergol. Int.*, vol. 61, no. 3, pp. 353–363, 2012.

[14] G. Shanthakumari and E. Priya, "Performance analysis: Preprocessing of respiratory lung sounds," in *Proc. Int. Conf. Sri Lanka Assoc. Artif. Intell.* Singapore: Springer, 2018, pp. 289–300.

[15] T. Elfaramawy, C. L. Fall, S. Arab, M. Morissette, F. Lellouche, and B. Gosselin, "A wireless respiratory monitoring system using a wearable patch sensor network," *IEEE Sensors J.*, vol. 19, no. 2, pp. 650–657, 2018.

[16] F. Ghulam Nabi, K. Sundaraj, L. Chee Kiang, R. Palaniappan, and S. Sundaraj, "Wheeze sound analysis using computer-based techniques: A systematic review," *Biomed. Eng. Biomed. Technik*, vol. 0, no. 0, pp. 1–28, Jan. 2017.

[17] Y. Yuasa, K. Takahashi, and K. Suzuki, "Wearable flexible device for respiratory phase measurement based on sound and chest movement," in *Proc. IEEE Int. Conf. Syst., Man, Cybern. (SMC)*, Oct. 2017, pp. 2378–2383.

[18] F. Nabi, K. Sundaraj, C. Lam, R. Palaniappan, and J. Hussain, "Recommendations related to wheeze sound data acquisition," *J. Telecommun., Electron. Comput. Eng.*, vol. 10, nos. 1–13, pp. 117–120, 2018.

[19] S.-H. Li, B.-S. Lin, C.-H. Tsai, C.-T. Yang, and B.-S. Lin, "Design of wearable breathing sound monitoring system for real-time wheeze detection," *Sensors*, vol. 17, no. 12, p. 171, Jan. 2017.

[20] P. Corbishley and E. Rodriguez-Villegas, "Breathing detection: Towards a miniaturized, wearable, battery-operated monitoring system," *IEEE Trans. Biomed. Eng.*, vol. 55, no. 1, pp. 196–204, Jan. 2008.

[21] A. Basra, B. Mukhopadhayay, and S. Kar, "Temperature sensor based ultra low cost respiration monitoring system," in *Proc. 9th Int. Conf. Commun. Syst. Netw. (COMSNETS)*, Jan. 2017, pp. 530–535.

[22] A. Agnihotri, "Human body respiration measurement using digital temperature sensor with i2c interface," *Int. J. Sci. Res.*, vol. 3, no. 3, pp. 1–8, 2013.

[23] S. Milici, J. Lorenzo, A. Lazaro, R. Villarino, and D. Girbau, "Wireless breathing sensor based on wearable modulated frequency selective surface," *IEEE Sensors J.*, vol. 17, no. 5, pp. 1285–1292, Mar. 2017.

[24] J. Lorenzo, A. Lazaro, R. Villarino, and D. Girbau, "Modulated frequency selective surfaces for wearable RFID and sensor applications," *IEEE Trans. Antennas Propag.*, vol. 64, no. 10, pp. 4447–4456, Oct. 2016.

[25] C.-L. Wei, Y.-C. Lin, T.-A. Chen, R.-Y. Lin, and T.-H. Liu, "Respiration detection chip with integrated temperature-insensitive MEMS sensors and CMOS signal processing circuits," *IEEE Trans. Biomed. Circuits Syst.*, vol. 9, no. 1, pp. 105–112, Feb. 2015.

[26] M.-K. Tsai, T.-A. Chen, H.-Y. Chiu, T.-W. Wu, and C.-L. Wei, "Monolithic airflow detection chip with automatic DC offset calibration," *IEEE Trans. Circuits Syst. I, Reg. Papers*, vol. 65, no. 1, pp. 107–117, Jan. 2018.

[27] C.-M. Yu, M.-K. Tsai, H.-Y. Chiu, and C.-L. Wei, "Single-battery-powered CMOS/MEMS respiration detection monolithic chip," in *Proc. IEEE Int. Symp. Circuits Syst. (ISCAS)*, May 2019, pp. 1–4.

[28] J. Jin and E. Sanchez-Sinencio, "A home sleep apnea screening device with time-domain signal processing and autonomous scoring capability," *IEEE Trans. Biomed. Circuits Syst.*, vol. 9, no. 1, pp. 96–104, Feb. 2015.

[29] C.-L. Wei, C.-F. Lin, and I.-T. Tseng, "A novel mems respiratory flow sensor," *IEEE Sensors J.*, vol. 10, no. 1, pp. 16–18, Dec. 2009.

[30] C. N. Brookes, "The PEP respiratory monitor: A validation study," *Emergency Med. J.*, vol. 20, no. 4, pp. 326–328, Jul. 2003.

[31] N. Donnelly *et al.*, "Demonstrating the accuracy of an in-hospital ambulatory patient monitoring solution in measuring respiratory rate," in *Proc. 35th Annu. Int. Conf. IEEE Eng. Med. Biol. Soc. (EMBC)*, Jul. 2013, pp. 6711–6715.

[32] C. Subbe and S. Kinsella, "Continuous monitoring of respiratory rate in emergency admissions: Evaluation of the respira sense sensor in acute care compared to the industry standard and gold standard," *Sensors*, vol. 18, no. 8, p. 2700, Aug. 2018.

[33] I. Kerslake and F. Kelly, "Uses of capnography in the critical care unit," *BJA Educ.*, vol. 17, no. 5, pp. 178–183, May 2017.

[34] O. P. Singh and M. Malarvili, "Review of infrared carbon-dioxide sensors and capnogram features for developing asthma-monitoring device," *J. Clin. DIAGNOSTIC Res.*, vol. 12, no. 10, pp. 1–6, 2018.

[35] S. Xiao *et al.*, "Fast-response ionogel humidity sensor for real-time monitoring of breathing rate," *Mater. Chem. Frontiers*, vol. 3, no. 3, pp. 484–491, 2019.

[36] S. Malik, M. Ahmad, M. Punjiya, A. Sadeqi, M. S. Baghini, and S. Sonkusale, "Respiration monitoring using a flexible paper-based capacitive sensor," in *Proc. IEEE SENSORS*, Dec. 2018, pp. 1–4.

[37] S. Kano, A. Yamamoto, A. Ishikawa, and M. Fujii, "Respiratory rate on exercise measured by nanoparticle-based humidity sensor," in *Proc. 41st Annu. Int. Conf. IEEE Eng. Med. Biol. Soc. (EMBC)*, Jul. 2019, pp. 3567–3570.

[38] S. Kano and M. Fujii, "Battery-powered wearable respiration sensor chip with nanocrystal thin film," in *Proc. IEEE SENSORS*, Oct. 2017, pp. 1–3.

[39] F. Gúder *et al.*, "Paper-based electrical respiration sensor," *Angew. Chem. Int. Ed.*, vol. 55, no. 19, pp. 5727–5732, May 2016.

[40] F. C. Favero, J. Villatoro, and V. Pruneri, "Microstructured optical fiber interferometric breathing sensor," *J. Biomed. Opt.*, vol. 17, no. 3, 2012, Art. no. 037006.

[41] J. Mathew, Y. Semenova, and G. Farrell, "A miniature optical breathing sensor," *Biomed. Opt. Exp.*, vol. 3, no. 12, pp. 3325–3331, 2012.

[42] A. M. Soomro, F. Jabbar, M. Ali, J.-W. Lee, S. W. Mun, and K. H. Choi, "All-range flexible and biocompatible humidity sensor based on poly lactic glycolic acid (PLGA) and its application in human breathing for wearable health monitoring," *J. Mater. Sci., Mater. Electron.*, vol. 30, no. 10, pp. 9455–9465, May 2019.

[43] Z. M. Rittersma, "Recent achievements in miniaturised humidity sensors—A review of transduction techniques," *Sens. Actuators A, Phys.*, vol. 96, nos. 2–3, pp. 196–210, Feb. 2002.

[44] I. Mahbub *et al.*, "A low-power wireless piezoelectric sensor-based respiration monitoring system realized in CMOS process," *IEEE Sensors J.*, vol. 17, no. 6, pp. 1858–1864, Mar. 2017.

[45] A. Richer and A. Adler, "Eddy current based flexible sensor for contactless measurement of breathing," in *Proc. IEEE Instrumentationand Meas. Technol. Conf. Proc.*, 2005, pp. 257–260.

[46] M. Steffen, A. Aleksandrowicz, and S. Leonhardt, "Mobile noncontact monitoring of heart and lung activity," *IEEE Trans. Biomed. Circuits Syst.*, vol. 1, no. 4, pp. 250–257, Dec. 2007.

[47] D. Teichmann, J. Foussier, and S. Leonhardt, "Respiration monitoring based on magnetic induction using a single coil," in *Proc. Biomed. Circuits Syst. Conf.*, Nov. 2010, pp. 37–40.

[48] S. Hwan Hwang *et al.*, "Unconstrained sleep apnea monitoring using polyvinylidene fluoride film-based sensor," *IEEE Trans. Biomed. Eng.*, vol. 61, no. 7, pp. 2125–2134, Jul. 2014.

[49] T. Elfaramawy, C. Latyr Fall, M. Morissette, F. Lellouche, and B. Gosselin, "Wireless respiratory monitoring and coughing detection using a wearable patch sensor network," in *Proc. 15th IEEE Int. New Circuits Syst. Conf. (NEWCAS)*, Jun. 2017, pp. 197–200.

[50] T. Reinvuo, M. Hannula, H. Sorvoja, E. Alasaarela, and R. Myllyla, "Measurement of respiratory rate with high-resolution accelerometer and emfit pressure sensor," in *Proc. IEEE Sensors Appl. Symp.*, Dec. 2006, pp. 192–195.

[51] P. D. Hung, S. Bonnet, R. Guillemaud, E. Castelli, and P. T. N. Yen, "Estimation of respiratory waveform using an accelerometer," in *Proc. 5th IEEE Int. Symp. Biomed. Imag., From Nano Macro*, May 2008, pp. 1493–1496.

[52] P. Jourand, H. De Clercq, R. Corthout, and R. Puers, "Textile integrated breathing and ECG monitoring system," *Procedia Chem.*, vol. 1, no. 1, pp. 722–725, Sep. 2009.

[53] A. Jin, B. Yin, G. Morren, H. Duric, and R. M. Aarts, "Performance evaluation of a tri-axial accelerometry-based respiration monitoring for ambient assisted living," in *Proc. Annu. Int. Conf. IEEE Eng. Med. Biol. Soc.*, Sep. 2009, pp. 5677–5680.

[54] A. Siqueira, A. F. Spirandeli, R. Moraes, and V. Zarzoso, "Respiratory waveform estimation from multiple accelerometers: An optimal sensor number and placement analysis," *IEEE J. Biomed. Health Informat.*, vol. 23, no. 4, pp. 1507–1515, Jul. 2019.

[55] A. Shahshahani, S. Bhadra, and Z. Zilic, "A continuous respiratory monitoring system using ultrasound piezo transducer," in *Proc. IEEE Int. Symp. Circuits Syst. (ISCAS)*, Oct. 2018, pp. 1–4.

[56] A. Shahshahani, C. Laverdiere, S. Bhadra, and Z. Zilic, "Ultrasound sensors for diaphragm motion tracking: An application in non-invasive respiratory monitoring," *Sensors*, vol. 18, no. 8, p. 2617, Aug. 2018.

[57] G. P. Heldt and R. J. Ward, "Evaluation of ultrasound-based sensor to monitor respiratory and nonrespiratory movement and timing in infants," *IEEE Trans. Biomed. Eng.*, vol. 63, no. 3, pp. 619–629, Mar. 2016.

[58] S. D. Min, D. J. Yoon, S. W. Yoon, Y. H. Yun, and M. Lee, "A study on a non-contacting respiration signal monitoring system using Doppler ultrasound," *Med. Biol. Eng. Comput.*, vol. 45, no. 11, pp. 1113–1119, Nov. 2007.

[59] A. Shahshahani, Z. Zilic, and S. Bhadra, "An ultrasound-based biomedical system for continuous cardiopulmonary monitoring: A single sensor for multiple information," *IEEE Trans. Biomed. Eng.*, vol. 67, no. 1, pp. 268–276, Jan. 2020.

[60] P. P. Tarjan and R. McFee, "Electrodeless measurements of the effective resistivity of the human torso and head by magnetic induction," *IEEE Trans. Biomed. Eng.*, vols. BME–15, no. 4, pp. 266–278, Oct. 1968.

[61] R. Seeton and A. Adler, "Sensitivity of a single coil electromagnetic sensor for non-contact monitoring of breathing," in *Proc. 30th Annu. Int. Conf. IEEE Eng. Med. Biol. Soc.*, Aug. 2008, pp. 518–521.

[62] F. Heydari, M. P. Ebrahim, and M. R. Yuce, "Chest-based real-time pulse and respiration monitoring based on bio-impedance," in *Proc. 42nd Annu. Int. Conf. IEEE Eng. Med. Biol. Soc. (EMBC)*, Jul. 2020, pp. 4398–4401.

[63] J. Moraes, M. Rocha, G. Vasconcelos, J. Vasconcelos Filho, V. de Albuquerque, and A. Alexandria, "Advances in photopletysmography signal analysis for biomedical applications," *Sensors*, vol. 18, no. 6, p. 1894, Jun. 2018.

[64] W. Karlen, S. Raman, J. M. Ansermino, and G. A. Dumont, "Multiparameter respiratory rate estimation from the photoplethysmogram," *IEEE Trans. Biomed. Eng.*, vol. 60, no. 7, pp. 1946–1953, Jul. 2013.

[65] L. M. Nilsson, "Respiration signals from photoplethysmography," *Anesthesia Analgesia*, vol. 117, no. 4, pp. 859–865, Oct. 2013.

[66] K. H. Shelley, A. A. Awad, R. G. Stout, and D. G. Silverman, "The use of joint time frequency analysis to quantify the effect of ventilation on the pulse oximeter waveform," *J. Clin. Monitor. Comput.*, vol. 20, no. 2, pp. 81–87, Jun. 2006.

[67] K. Nakajima, T. Tamura, and H. Miike, "Monitoring of heart and respiratory rates by photoplethysmography using a digital filtering technique," *Med. Eng. Phys.*, vol. 18, no. 5, pp. 365–372, Jul. 1996.

[68] P. Leonard, N. R. Grubb, P. S. Addison, D. Clifton, and J. N. Watson, "An algorithm for the detection of individual breaths from the pulse oximeter waveform," *J. Clin. Monitor. Comput.*, vol. 18, nos. 5–6, pp. 309–312, Dec. 2004.

[69] K. H. Chon, S. Dash, and K. Ju, "Estimation of respiratory rate from photoplethysmogram data using time–frequency spectral estimation," *IEEE Trans. Biomed. Eng.*, vol. 56, no. 8, pp. 2054–2063, Aug. 2009.

[70] S. G. Fleming and L. Tarassenko, "A comparison of signal processing techniques for the extraction of breathing rate from the photoplethysmogram," *Int. J. Biol. Med. Sci.*, vol. 2, no. 4, pp. 232–236, 2007.

[71] P. H. Charlton, T. Bonnici, L. Tarassenko, D. A. Clifton, R. Beale, and P. J. Watkinson, "An assessment of algorithms to estimate respiratory rate from the electrocardiogram and photoplethysmogram," *Physiol. Meas.*, vol. 37, no. 4, p. 610, 2016.

[72] R. Bailon, L. Sornmo, and P. Laguna, "A robust method for ECG-based estimation of the respiratory frequency during stress testing," *IEEE Trans. Biomed. Eng.*, vol. 53, no. 7, pp. 1273–1285, Jul. 2006.

[73] R. Pallas-Areny, J. Colominas-Balague, and F. J. Rosell, "The effect of respiration-induced heart movements on the ECG," *IEEE Trans. Biomed. Eng.*, vol. 36, no. 6, pp. 585–590, Jun. 1989.

[74] P. de Chazal, C. Heneghan, E. Sheridan, R. Reilly, P. Nolan, and M. O'Malley, "Automated processing of the single-lead electrocardiogram for the detection of obstructive sleep apnoea," *IEEE Trans. Biomed. Eng.*, vol. 50, no. 6, pp. 686–696, Jun. 2003.

[75] W. J. Yi and K. S. Park, "Derivation of respiration from ECG measured without subject's awareness using wavelet transform," in *Proc. 24th Annu. Conf. Annu. Fall Meeting Biomed. Eng.*, 2002, pp. 130–131.

[76] S. Dash, K. H. Shelley, D. G. Silverman, and K. H. Chon, "Estimation of respiratory rate from ECG, photoplethysmogram, and piezoelectric pulse transducer signals: A comparative study of time–frequency methods," *IEEE Trans. Biomed. Eng.*, vol. 57, no. 5, pp. 1099–1107, May 2010.

[77] O. Meste, G. Blain, and S. Bermon, "Analysis of the respiratory and cardiac systems coupling in pyramidal exercise using a time-varying model," in *Proc. Comput. Cardiol.*, 2002, pp. 429–432.

[78] C. B. Pereira, X. Yu, M. Czaplik, R. Rossaint, V. Blazek, and S. Leonhardt, "Remote monitoring of breathing dynamics using infrared thermography," *Biomed. Opt. Exp.*, vol. 6, no. 11, pp. 4378–4394, 2015.

[79] N. Otsu, "A threshold selection method from gray-level histograms," *IEEE Trans. Syst., Man, Cybern.*, vol. SMC-9, no. 1, pp. 62–66, Jan. 1979.

[80] F. Q. AL-Khalidi, R. Saatchi, D. Burke, and H. Elphick, "Facial tracking method for noncontact respiration rate monitoring," in *Proc. 7th Int. Symp. Commun. Syst., Netw. Digit. Signal Process. (CSNDSP)*, Jul. 2010, pp. 751–754.

[81] C. B. Pereira, X. Yu, V. Blazek, and S. Leonhardt, "Robust remote monitoring of breathing function by using infrared thermography," in *Proc. 37th Annu. Int. Conf. IEEE Eng. Med. Biol. Soc. (EMBC)*, Aug. 2015, pp. 4250–4253.

[82] X. Mei and H. Ling, "Robust visual tracking and vehicle classification via sparse representation," *IEEE Trans. Pattern Anal. Mach. Intell.*, vol. 33, no. 11, pp. 2259–2272, Nov. 2011.

[83] A. Procházka, H. Charvátová, O. Vyáata, J. Kopal, and J. Chambers, "Breathing analysis using thermal and depth imaging camera video records," *Sensors*, vol. 17, no. 6, p. 1408, Jun. 2017.

[84] L. Boccanfuso and J. M. O'Kane, "Remote measurement of breathing rate in real time using a high precision, single-point infrared temperature sensor," in *Proc. 4th IEEE RAS EMBS Int. Conf. Biomed. Robot. Biomechtron. (BioRob)*, Jun. 2012, pp. 1704–1709.

[85] C. Bruser, S. Winter, and S. Leonhardt, "How speech processing can help with beat-to-beat heart rate estimation in ballistocardiograms," in *Proc. IEEE Int. Symp. Med. Meas. Appl. (MeMeA)*, May 2013, pp. 12–16.

[86] K. Mutlu, J. E. Rabell, P. Martin del Olmo, and S. Haesler, "IR thermography-based monitoring of respiration phase without image segmentation," *J. Neurosci. Methods*, vol. 301, pp. 1–8, May 2018.

[87] K. Nakajima, Y. Matsumoto, and T. Tamura, "Development of real-time image sequence analysis for evaluating posture change and respiratory rate of a subject in bed," *Physiol. Meas.*, vol. 22, no. 3, pp. N21–N28, Aug. 2001.

[88] I. Sato and M. Nakajima, "Non-contact breath motion monitor ing system in full automation," in *Proc. 27th Annu. Conf. Eng. Med. Biol.*, Dec. 2005, pp. 3448–3451.

[89] J. Penne, C. Schaller, J. Hornegger, and T. Kuwert, "Robust real-time 3D respiratory motion detection using time-of-flight cameras," *Int. J. Comput. Assist. Radiol. Surgery*, vol. 3, no. 5, pp. 427–431, Nov. 2008.

[90] N. Bernacchia, L. Scalise, L. Casacanditella, I. Ercoli, P. Marchionni, and E. P. Tomasini, "Non contact measurement of heart and respiration rates based on Kinect," in *Proc. IEEE Int. Symp. Med. Meas. Appl. (MeMeA)*, Jun. 2014, pp. 1–5.

[91] M. Bartula, T. Tigges, and J. Muehlsteff, "Camera-based system for contactless monitoring of respiration," in *Proc. 35th Annu. Int. Conf. IEEE Eng. Med. Biol. Soc. (EMBC)*, Jul. 2013, pp. 2672–2675.

[92] A. Al-Naji, K. Gibson, S.-H. Lee, and J. Chahl, "Monitoring of cardiorespiratory signal: Principles of remote measurements and review of methods," *IEEE Access*, vol. 5, pp. 15776–15790, 2017.

[93] A. P. Prathosh, P. Praveena, L. K. Mestha, and S. Bharadwaj, "Estimation of respiratory pattern from video using selective ensemble aggregation," *IEEE Trans. Signal Process.*, vol. 65, no. 11, pp. 2902–2916, Jun. 2017.

[94] C. Li, X. Yu, C.-M. Lee, D. Li, L. Ran, and J. Lin, "High-sensitivity software-configurable 5.8-GHz radar sensor receiver chip in 0.13 μm CMOS for noncontact vital sign detection," *IEEE Trans. Microw. Theory Techn.*, vol. 58, no. 5, pp. 1410–1419, 2010.

[95] D. Zito, D. Pepe, M. Mincica, and F. Zito, "A 90 nm CMOS SoC UWB pulse radar for respiratory rate monitoring," in *Proc. IEEE Int. Solid-State Circuits Conf.*, Feb. 2011, pp. 40–41.

[96] X. Gao, A. Singh, E. Yavari, V. Lubecke, and O. Boric-Lubecke, "Non-contact displacement estimation using Doppler radar," in *Proc. Annu. Int. Conf. IEEE Eng. Med. Biol. Soc.*, Aug. 2012, pp. 1602–1605.

[97] B.-K. Park, O. Boric-Lubecke, and V. M. Lubecke, "Arctangent demodulation with DC offset compensation in quadrature Doppler radar receiver systems," *IEEE Trans. Microw. Theory Techn.*, vol. 55, no. 5, pp. 1073–1079, May 2007.

[98] T.-Y.-J. Kao, Y. Yan, T.-M. Shen, A. Y.-K. Chen, and J. Lin, "Design and analysis of a 60-GHz CMOS Doppler micro-radar system-in-package for vital-sign and vibration detection," *IEEE Trans. Microw. Theory Techn.*, vol. 61, no. 4, pp. 1649–1659, Apr. 2013.

[99] C. Li, Y. Xiao, and J. Lin, "A 5 GHz double-sideband radar sensor chip in 0.18 μm CMOS for non-contact vital sign detection," *IEEE Microw. Wireless Compon. Lett.*, vol. 18, no. 7, pp. 494–496, 2008.

[100] A. D. Droitcour, O. Boric-Lubecke, V. M. Lubecke, and J. Lin, "0.25 μm CMOS and BiCMOS single-chip direct-conversion Doppler radar for remote sensing of vital signs," in *IEEE Int. Solid-State Circuits Conf. (ISSCC) Dig. Tech. Papers*, 2002, pp. 348–349.

[101] A. D. Droitcour, O. Boric-Lubecke, and G. T. A. Kovacs, "Signal-to-noise ratio in Doppler radar system for heart and respiratory rate measurements," *IEEE Trans. Microw. Theory Techn.*, vol. 57, no. 10, pp. 2498–2507, Oct. 2009.

[102] H.-C. Kuo *et al.*, "A fully integrated 60-GHz CMOS direct-conversion Doppler radar RF sensor with clutter canceller for single-antenna noncontact human vital-signs detection," *IEEE Trans. Microw. Theory Techn.*, vol. 64, no. 4, pp. 1018–1028, Apr. 2016.

[103] C.-C. Chou, W.-C. Lai, Y.-K. Hsiao, and H.-R. Chuang, "60-GHz CMOS Doppler radar sensor with integrated V-band power detector for clutter monitoring and automatic clutter-cancellation in noncontact vital-signs sensing," *IEEE Trans. Microw. Theory Techn.*, vol. 66, no. 3, pp. 1635–1643, Dec. 2017.

[104] J. H. Choi and D. K. Kim, "A remote compact sensor for the real-time monitoring of human heartbeat and respiration rate," *IEEE Trans. Biomed. Circuits Syst.*, vol. 3, no. 3, pp. 181–188, Jun. 2009.

[105] P.-H. Wu, F.-H. Chung, and P. Hsu, "A 5.8 GHz phase- and self-injection-locked CMOS radar sensor chip for vital sign detector miniaturization," in *IEEE MTT-S Int. Microw. Symp. Dig.*, May 2016, pp. 1–3.

[106] C. Li, V. M. Lubecke, O. Boric-Lubecke, and J. Lin, "A review on recent advances in Doppler radar sensors for noncontact healthcare monitoring," *IEEE Trans. Microw. Theory Techn.*, vol. 61, no. 5, pp. 2046–2060, May 2013.

[107] L. Scalise, P. Marchionni, I. Ercoli, and E. P. Tomasini, "Simultaneous measurement of respiration and cardiac period in preterm infants by laser Doppler vibrometry," *AIP Conf. Proc.*, vol. 1457, no. 1, pp. 275–281, 2012.

[108] L. Scalise, P. Marchionni, and I. Ercoli, "Non-contact laser-based human respiration rate measurement," *AIP Conf. Proc.*, vol. 1364, pp. 149–155, Dec. 2011.

[109] L. Scalise, P. Marchionni, and I. Ercoli, "Optical method for measurement of respiration rate," in *Proc. IEEE Int. Workshop Med. Meas. Appl.*, Dec. 2010, pp. 19–22.

[110] L. Scalise, I. Ercoli, P. Marchionni, and E. P. Tomasini, "Measurement of respiration rate in preterm infants by laser Doppler vibrometry," in *Proc. IEEE Int. Symp. Med. Meas. Appl.*, Mar. 2011, pp. 657–661.

[111] J. Kranjec, S. Begušš, G. Geršak, and J. Drnovšek, "Non-contact heart rate and heart rate variability measurements: A review," *Biomed. Signal Process. Control*, vol. 13, pp. 102–112, Sep. 2014.

[112] H. Lee, B.-H. Kim, J.-K. Park, S. W. Kim, and J.-G. Yook, "A resolution enhancement technique for remote monitoring of the vital signs of multiple subjects using a 24 GHz bandwidth-limited FMCW radar," *IEEE Access*, vol. 8, pp. 1240–1248, 2020.

[113] D. Zito *et al.*, "SoC CMOS UWB pulse radar sensor for contactless respiratory rate monitoring," *IEEE Trans. Biomed. Circuits Syst.*, vol. 5, no. 6, pp. 503–510, Dec. 2011.

[114] X. Wang, A. Dinh, and D. Teng, "3–10 GHz ultra wideband front-end transceiver in 0.13 μm complementary metal oxide semiconductor for low-power biomedical radar," *IET Circuits, Devices Syst.*, vol. 8, no. 4, pp. 272–279, Jul. 2014.

[115] T.-S. Chu, J. Roderick, S. Chang, T. Mercer, C. Du, and H. Hashemi, "A short-range UWB impulse-radio CMOS sensor for human feature detection," in *Proc. IEEE Int. Solid-State Circuits Conf.*, Feb. 2011, pp. 294–296.

[116] D. T. Wisland, K. Granhaug, J. R. Pleym, N. Andersen, S. Stoa, and H. A. Hjortland, "Remote monitoring of vital signs using a CMOS UWB radar transceiver," in *Proc. 14th IEEE Int. New Circuits Syst. Conf. (NEWCAS)*, Jun. 2016, pp. 1–4.

[117] C.-M. Lai, J.-M. Wu, P.-C. Huang, and T.-S. Chu, "A scalable direct-sampling broadband radar receiver supporting simultaneous digital multibeam array in 65nm CMOS," in *IEEE Int. Solid-State Circuits Conf. (ISSCC) Dig. Tech. Papers*, Feb. 2013, pp. 242–243.

[118] P. Park, S. Kim, S. Woo, and C. Kim, "A centimeter resolution, 10 μm range CMOS impulse radio radar for human motion monitoring," *IEEE J. Solid-State Circuits*, vol. 49, no. 5, pp. 1125–1134, May 2014.

[119] N. Andersen *et al.*, "A 118-mw pulse-based radar soc in 55-nm CMOS for non-contact human vital signs detection," *IEEE J. Solid-State Circuits*, vol. 52, no. 12, pp. 3421–3433, 2017.
[120] N. Andersen *et al.*, "A 118-mW 23.3-GS/s dual-band 7.3-GHz and 8.7-GHz impulse-based direct RF sampling radar SoC in 55-nm CMOS," in *IEEE Int. Solid-State Circuits Conf. (ISSCC) Dig. Tech. Papers*, Feb. 2017, pp. 138–139.
[121] S.-H. Yu and T.-S. Horng, "Highly linear phase-canceling self-injection-locked ultrasonic radar for non-contact monitoring of respiration and heartbeat," *IEEE Trans. Biomed. Circuits Syst.*, vol. 14, no. 1, pp. 75–90, Feb. 2020.
[122] M. Ali, H. Shawkey, A. Zekry, and M. Sawan, "One mbps 1 nJ/b 3.5–4 GHz fully integrated FM-UWB transmitter for WBAN applications," *IEEE Trans. Circuits Syst. I, Reg. Papers*, vol. 65, no. 6, pp. 2005–2014, Jun. 2018.
[123] B. Schleicher, I. Nasr, A. Trasser, and H. Schumacher, "IR-UWB radar demonstrator for ultra-fine movement detection and vital-sign monitoring," *IEEE Trans. Microw. Theory Techn.*, vol. 61, no. 5, pp. 2076–2085, May 2013.
[124] H. G. Han, B. G. Yu, and T. W. Kim, "A 1.9-mm-precision 20-GHz direct-sampling receiver using time-extension method for indoor localization," *IEEE J. Solid-State Circuits*, vol. 52, no. 6, pp. 1509–1520, Jun. 2017.
[125] H. A. Hjortland, D. T. Wisland, T. S. Lande, C. Limbodal, and K. Meisal, "Thresholded samplers for UWB impulse radar," in *Proc. IEEE Int. Symp. Circuits Syst.*, May 2007, pp. 1210–1213.
[126] K. van Loon *et al.*, "Wireless non-invasive continuous respiratory monitoring with FMCW radar: A clinical validation study," *J. Clin. Monitor. Comput.*, vol. 30, no. 6, pp. 797–805, Dec. 2016.
[127] C. Uysal and T. Filik, "RF-based noncontact respiratory rate monitoring with parametric spectral estimation," *IEEE Sensors J.*, vol. 19, no. 21, pp. 9841–9849, Nov. 2019.
[128] D. Zhang, M. Kurata, and T. Inaba, "FMCW radar for small displacement detection of vital signal using projection matrix method," *Int. J. Antennas Propag.*, vol. 2013, pp. 1–5, 2013.
[129] C. Gu *et al.*, "An instruments-built Doppler radar for sensing vital signs," in *Proc. 8th Int. Symp. Antennas, Propag. EM Theory*, 2008, pp. 1398–1401.
[130] A. Tariq and H. Ghafouri-Shiraz, "Vital signs detection using Doppler radar and continuous wavelet transform," in *Proc. 5th Eur. Conf. Antennas Propag. (EUCAP)*, Dec. 2011, pp. 285–288.
[131] N. Birsan, D.-P. Munteanu, G. Iubu, and T. Niculescu, "Time-frequency analysis in Doppler radar for noncontact cardiopulmonary monitoring," in *Proc. E-Health Bioengineering Conf. (EHB)*, 2011, pp. 1–4.
[132] R. Ravichandran, E. Saba, K.-Y. Chen, M. Goel, S. Gupta, and S. N. Patel, "WiBreathe: Estimating respiration rate using wireless signals in natural settings in the home," in *Proc. IEEE Int. Conf. Pervas. Comput. Commun. (PerCom)*, Mar. 2015, pp. 131–139.
[133] Y. S. Lee, P. N. Pathirana, C. L. Steinfort, and T. Caelli, "Monitoring and analysis of respiratory patterns using microwave Doppler radar," *IEEE J. Translational Eng. Health Med.*, vol. 2, pp. 1–12, 2014.
[134] T. Taheri and A. Sant'Anna, "Non-invasive breathing rate detection using a very low power ultra-wide-band radar," in *Proc. IEEE Int. Conf. Bioinf. Biomed. (BIBM)*, Nov. 2014, pp. 78–83.
[135] A. Q. Javaid, C. M. Noble, R. Rosenberg, and M. A. Weitnauer, "Towards detection of sleep apnea events by combining different non-contact measurement modalities," in *Proc. 38th Annu. Int. Conf. IEEE Eng. Med. Biol. Soc. (EMBC)*, Aug. 2016, pp. 5307–5310.
[136] V. C. Chen, *The Micro-Doppler Effect Radar*. Norwood, MA, USA: Artech House, 2019.
[137] A. Al-Naji, A. J. Al-Askery, S. K. Gharghan, and J. Chahl, "A system for monitoring breathing activity using an ultrasonic radar detection with low power consumption," *J. Sensor Actuator Netw.*, vol. 8, no. 2, p. 32, May 2019.
[138] P. Arlotto, M. Grimaldi, R. Naeck, and J.-M. Ginoux, "An ultrasonic contactless sensor for breathing monitoring," *Sensors*, vol. 14, no. 8, pp. 15371–15386, 2014.
[139] P. I. Terrill, S. J. Wilson, S. Suresh, D. M. Cooper, and C. Dakin, "Application of recurrence quantification analysis to automatically estimate infant sleep states using a single channel of respiratory data," *Med. Biol. Eng. Comput.*, vol. 50, no. 8, pp. 851–865, Aug. 2012.
[140] W. Karlen, J. Lim, J. M. Ansermino, G. Dumont, and C. Scheffer, "Design challenges for camera oximetry on a mobile phone," in *Proc. Annu. Int. Conf. IEEE Eng. Med. Biol. Soc.*, Aug. 2012, pp. 2448–2451.
[141] J. Lázaro, Y. Nam, E. Gil, P. Laguna, and K. H. Chon, "Respiratory rate derived from smartphone-camera-acquired pulse photoplethysmographic signals," *Physiol. Meas.*, vol. 36, no. 11, p. 2317, 2015.
[142] M. van Gastel, S. Stuijk, and G. de Haan, "Robust respiration detection from remote photoplethysmography," *Biomed. Opt. Exp.*, vol. 7, no. 12, pp. 4941–4957, 2016.
[143] W. Karlen, A. Garde, D. Myers, C. Scheffer, J. M. Ansermino, and G. A. Dumont, "Estimation of respiratory rate from photoplethysmographic imaging videos compared to pulse oximetry," *IEEE J. Biomed. Health Informat.*, vol. 19, no. 4, pp. 1331–1338, Jul. 2015.
[144] R. Feger, A. Haderer, S. Schuster, S. Scheiblhofer, and A. Stelzer, "A four channel 24-GHz FMCW radar sensor with two-dimensional target localization capabilities," in *IEEE MTT-S Int. Microw. Symp. Dig.*, Jun. 2008, pp. 125–128.

Mohamed Ali (Member, IEEE) received the B.Sc. degree in electronics from the Faculty of Electronics Engineering, Menoufia University, Egypt, in 2005, the M.Sc. degree in electronics and communication engineering from Ain Shams University, Egypt, in 2011, and the Ph.D. degree in electronics and communication engineering from Ain Shams University, jointly with the Polytechnique Montréal, Montreal, QC, Canada, in 2017. He joined the Polytechnique Montréal as a Research Intern from 2015 to 2017 as a part of his Ph.D. program. Since 2007, he has been with the Microelectronics Department, Electronics Research Institute, Giza, Egypt. He is a Postdoctoral Fellow with the Department of Electrical Engineering, Polytechnique Montréal. His current research interests include analog, RF, and mixed-signal design.

Ali Elsayed received the B.Sc. degree in nanotechnology and nanoelectronics from the Zewail City of Science, Technology and Innovation, Egypt, in 2019. He is currently pursuing the master's degree with the Erasmus Mundus Master on Innovative Microwave Electronics and Optics (EMIMEO). He has participated in multiple research projects, notably in Cairo University, Egypt, in 2017 on modelling Triboelectric Nanogenerators and in the Polytechnic Montréal, Canada, in 2018 on the use and design of compact medical sensors. His research interests include new generation of photonics and their use in communication systems.

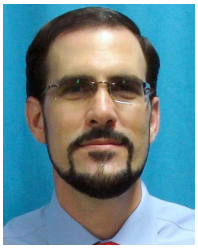

Arnaldo Mendez (Member, IEEE) received the bachelor's degree in computer engineering and the M.Sc. degree in automation science from the Polytechnique University of Havana, Cuba, and the Ph.D. degree in biomedical engineering from the École Polytechnique de Montréal, Montreal, QC, Canada. He was a Professor and the Chair of the Electronic Engineering Department, Universidad Autónoma de Occidente, Cali, Colombia. He was a Principal Engineer and the Head of the section of automatized micro-ELISA washers and dispensers in the Immunoassay-Research Center (Tecnosuma S.A.), Havana, Cuba. He is currently the Scientific Assistant of the Microsystems Strategic Alliance of Quebec (ReSMiQ), Montreal. He is also with the Department of Electrical Engineering as a Lecturer for courses in microelectronics and in smart medical devices in the École Polytechnique de Montréal. His research interests include smart prosthetic devices, embedded AI algorithms, mixed-signal integrated circuits, and the design and development of biomedical systems.

Yvon Savaria (Fellow, IEEE) received the B.Ing. and M.Sc.A. degrees in electrical engineering from the École Polytechnique de Montréal in 1980 and 1982, respectively, and the Ph.D. degree in electrical engineering from McGill University in 1985. Since 1985, he has been with the Polytechnique Montréal, where he is currently a Professor with the Department of Electrical Engineering. He is also affiliated with the Hangzhou Innovation Institute, Beihang University. He has carried out work in several areas related to microelectronic circuits and microsystems, such as testing, verification, validation, clocking methods, defect and fault tolerance, effects of radiation on electronics, high-speed interconnects and circuit design techniques, CAD methods, reconfigurable computing and applications of microelectronics to telecommunications, aerospace, image processing, video processing, radar signal processing, and the acceleration of digital signal processing. He is also involved in several projects related to embedded systems in aircraft, radiation effects on electronics, asynchronous circuit design and testing, green IT, wireless sensor networks, virtual networks, software-defined networks, machine learning, computational efficiency, and application-specific architecture design. He holds 16 patents, has published 150 journal articles and 450 conference papers, and was the thesis advisor of 160 graduate students who completed their studies. He was the Program Co-Chairman of NEWCAS'2018. He has been working as a Consultant or was sponsored for carrying out research by Bombardier, CNRC, Design Workshop, DREO, Ericsson, Genesis, Gennum, Huawei, Hyperchip, ISR, Kaloom, LTRIM, Miranda, MiroTech, Nortel, Octasic, PMC-Sierra, Technocap, Thales, Tundra, and Wavelite. He is a member of the Regroupement Stratégique en Microélectronique du Québec (RESMIQ), the Ordre des Ingénieurs du Québec (OIQ), and the CMC Microsystems Board. In 2001, he was awarded a Tier 1 Canada Research Chair (www.chairs.gc.ca) on the designs and architectures of advanced microelectronic systems that he held until June 2015. He received a Synergy Award of the Natural Sciences and Engineering Research Council of Canada in 2006.

Mohamad Sawan (Fellow, IEEE) received the Ph.D. degree in electrical engineering from Sherbrooke University, Canada, in 1990. He is a Chair Professor Founder and the Director of the Center for Biomedical Research and INnovation (CenBRAIN) and the Head of the Electrical Engineering Division, School of Engineering, Westlake University, Hangzhou, China. He is the Emeritus Professor of Microelectronics and Biomedical Engineering. He is the Founder and the Director of the Polystim Neurotech Laboratory, Polytechnique Montréal. He was leading the Microsystems Strategic Alliance of Quebec (ReSMiQ) from 1991 to 2019. He supervised the thesis of more than 120 master's and 60 Ph.D. students. He has published more than 800 peer-reviewed articles. He awarded 12 patents and 13 other patents are pending. Dr. Sawan is the Vice-President Publications since 2019 of the IEEE CAS Society. He is a Fellow of the Canadian Academy of Engineering and the Engineering Institute of Canada, and the Officer of the Quebec's National Order. He received several awards, among them the Queen Elizabeth II Golden Jubilee Medal, the Shanghai International Collaboration Award, the Bombardier Award for technology transfer, the Jacques-Rousseau Award, the medal of merit from the President of Lebanon, and the Barbara Turnbull Award for spinal cord research in Canada. He is/was the Founder of the Interregional IEEE NEWCAS Conference, and the Co-Founder and the Editor-in-Chief of the IEEE TRANSACTIONS ON BIOMEDICAL CIRCUITS AND SYSTEMS from 2016 to 2019.